2015

Deterministic and stochastic inversion techniques used to predict porosity: A case study from F3-Block

Hao Wu
Michigan Technological University, hwu4@mtu.edu

DETERMINISTIC AND STOCHASTIC INVERSION TECHNIQUES USED TO PREDICT POROSITY: A CASE STUDY FROM F3-BLOCK

By

Hao Wu

A THESIS

Submitted in partial fulfillment of the requirements for the degree of

MASTER OF SCIENCE

In Geophysics

MICHIGAN TECHNOLOGICAL UNIVERSITY

2015

This thesis has been approved in partial fulfillment of the requirements for the Degree of MASTER OF SCIENCE in Geophysics.

Department of Geological and Mining Engineering and Science

Thesis Advisor: *Wayne D. Pennington*

Committee Member: *Gregory P. Waite*

Committee Member: *Mir Sadri*

Department Chair: *John S. Gierke*

Table of Contents

Acknowledgement

My deepest gratitude is to my advisor Prof. Wayne D. Pennington for the support and patience of my Master's study and research, I would never finish this thesis without his guidance and encouragement.

I would like to thank Professor Gregory P. Waite. He is one of the best teachers that I have had in my life. He has opened a door for me, without taking the course of inverse theory that he taught, I would not have chosen seismic inversion as my thesis topic.

I would also like to thank Professor Mir Sadri. He always willing to help and give his best suggestions.

I am grateful to Dr. Bo Zhang for his encouragement and practical advice.

I want to thank the Opendtect (dGB Earth Science) who provided the data of the F3 Block.

The last but the most important, I would like to thank my parents, Lijun Wu and Huanzhang Wang. Thanks for your unconditional love when I feel down about my life.

Abstract

Within large-scale sigmoidal bedding of the F3-block in the shallow zone there appear to be some indicators of hydrocarbon deposits. In order to characterize target zone in the sigmoidal bedding, I combine the analysis of inverted results of post-stack seismic data with rock-physics relationships developed from well log data to predict the porosity, which ranges from 20% to 33%, for different system tracts in this area. The methods used in this study include conventional deterministic inversion and novel stochastic inversion. Through a rock physics analysis of the density, velocity and gamma-ray logs in two wells, I constructed relationships between the acoustic impedance and porosity; one is appropriate for the high-stand (more shale-prone) system tract, and one for the low-stand (more sand-prone) system tract. With the help of these two inversion methods and the two impedance-porosity relationships, four high-resolution porosity models have been generated providing insight into potential high-porosity and potential hydrocarbon-bearing zones.

1. Introduction

The main role of seismic data has been to identify the structure of the reflectors and detect their depth. But the various reflection amplitudes of the seismic trace are caused by the contrast of acoustic impedance at interfaces between different layers; acoustic impedance is the product of density and velocity (Barclay, 2008). By applying seismic inversion, which combines seismic data with well logs, we estimate the acoustic impedance throughout the whole seismic volume, rather than simply using the original seismic image.

Inversion can be considered as the analysis of data using forward modeling (Figure 1.1). In this study, the forward modeling starts with the product of bulk density and sonic velocity, which are obtained from well logs, and which can generate reflection coefficient. Reflection coefficient is the ratio of reflected amplitude and incident amplitude:

$$reflection\ coefficient = \frac{Reflected\ amplitude}{Incident\ amplitude} = \frac{V_1\rho_1 - V_2\rho_2}{V_1\rho_1 + V_2\rho_2}$$

Where $V_1\rho_1$ is the acoustic impedance of the first layer and $V_2\rho_2$ is the acoustic impedance of the second layer; V is the P-wave velocity, and ρ is the density.

We first convert the reflectivity measured at each depth (from the well logs) to two-way travel time, through the velocity measured in logs. We then convolve this reflectivity series with a wavelet to create a synthetic trace, as a routine part of seismic-well tie construction. Then we apply

seismic inversion, which starts with the real seismic data, applying methods using forward modeling to create a model of the earth that result in synthetic seismic data that looks like the real data. If done correctly, the model should closely resemble the earth (Barclay, 2008).

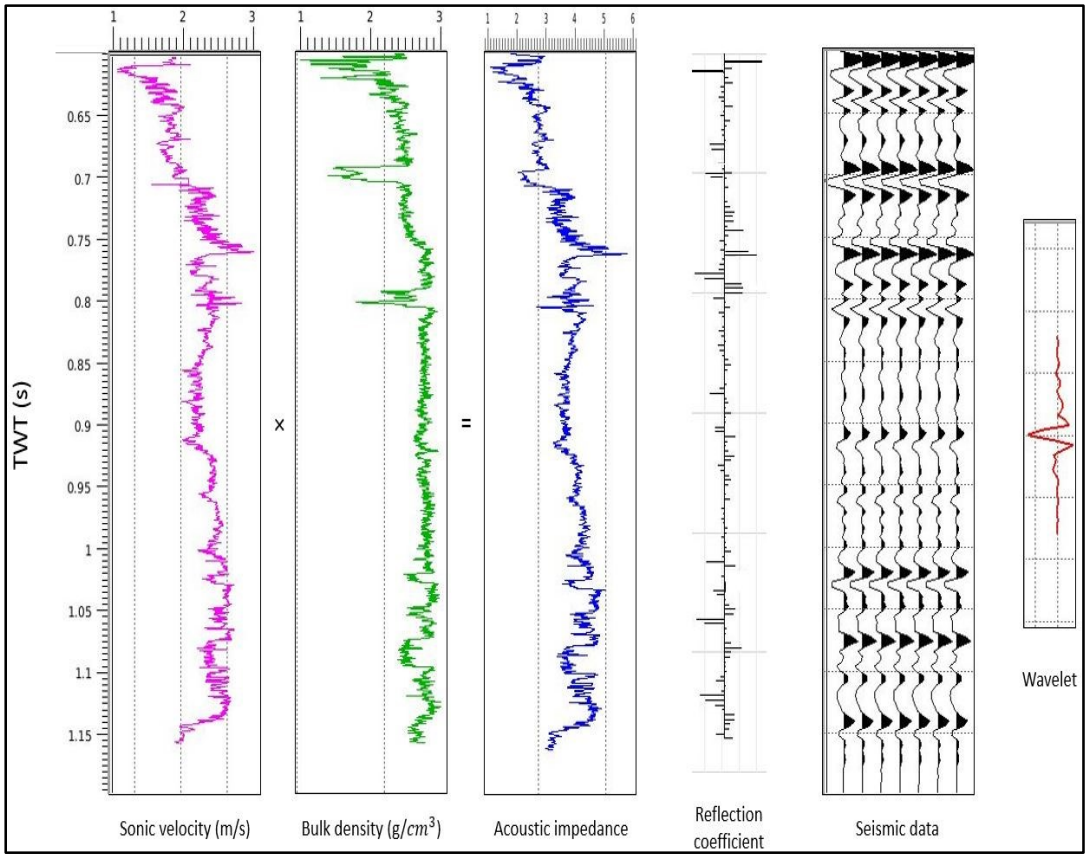

Figure 1.1. Forward modeling: simulate the reflection seismic data in the earth with different physical properties.

In this study, we applied two methods of inversion, deterministic inversion and stochastic inversion, to predict the porosity of the target zone. Both deterministic and stochastic inversion procedures in this study are model-based, and minimize the error between the synthetic seismogram and the input seismic data (Francis, 2005). The input seismic data are post-stack, while the physical property model being sought is acoustic impedance. Then, physical relationships will be applied to relate that impedance to porosity.

Figure 1.2 shows the workflow for the deterministic inversion. It is an iterative procedure that proceeds in the clockwise direction in Figure 1.2. We need to provide an initial impedance model and the far-field source wavelet. Convolution of this model and wavelet produces a trace (Cooke and Cant, 2010).

The next step is find the error between the synthetic trace and the input seismic trace through simple subtraction, and evaluate that error. If the error is not small enough to meet the exit threshold, we need to update our impedance model until the exit threshold is finally met. Then, the inversion processer will move to the next seismic trace and continue processing this procedure till the whole volume of the seismic data is done (Cooke and Cant, 2010). The final result is the deterministic inversion model.

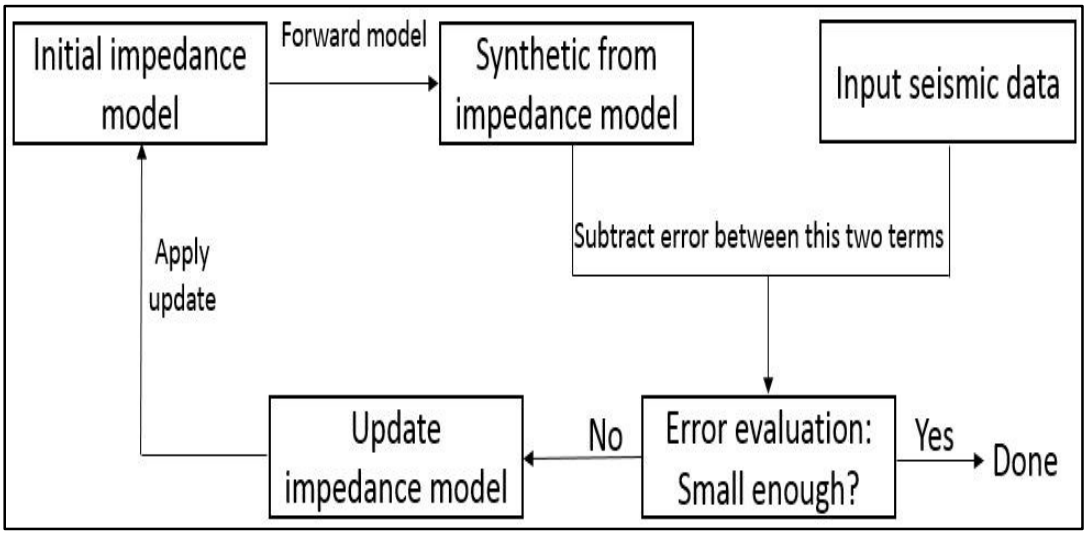

Figure 1.2. Iterative procedure of the model-based inversion.

Our seismic data is band-limited, and ranges from 8Hz to 80Hz. Lack of the high-frequency part will reduce the resolution of seismic data (Xi, 2013). Likewise, lack of the low-frequency part will result in an inability to recover slow changes in elastic properties at these long wavelengths. This means that in order to obtain the absolute acoustic impedance value, the low frequency model must be incorporated with well logs.

This low frequency model will be merged with the initial seismic-based impedance model. The lowest frequencies come from the interpolated values, while the frequencies within the seismic wavelet come from the inversion results. But we will have a non-unique solution, which means the value is based on the algorithm instead of depending on the physical property, if the frequency of synthetic seismogram is not within the wavelet (Francis, 2005). The role of judgment of the interpreter conducting the inversion is critical; it is necessary to be able to recognize

what results are constrained by the data, and what results are artifacts introduced by the process.

Deterministic seismic inversion has a significant limitation: deterministic inversion generates average impedances of each layer, and the range of values is smaller than the impedance from the wells. That is, the inversion will not produce results that are not within the calibration range. But according to geostatistical analysis, seismic inversion could calculate multiple possible simulations. This is done by conditioning well data and approximately reproducing spatially varying statistics (using what is called a variogram) which can overcome the limitation of band-limited deterministic seismic inversion (Francis 2005). This is the basis of the second type of inversion used in this study: stochastic inversion. Unlike deterministic seismic inversion, the stochastic method accounts for non-uniqueness of the inversion process by delivering multiple realizations that are matched with the available well and seismic data.

With the help of multiple realizations of acoustic impedance, we can use the inversion model in the reservoir characterization (Moyen and Doyen, 2009). The cross-plot of impedance against other physical properties like porosity and lithology can be done to estimate the uncertainty of the reservoir by invert the inversion models.

2. Regional geology and data summary

The data of this study is locate in the F3-block of the North Sea , which was provided by OpendTect (dGB Earth Science) including four vertical wells and one 3D seismic data set. All four wells have gamma ray and sonic logs, but only two wells have density logs.

Our target area is the apparent sigmoidal bedding in the shallow zone which located around 500ms to 1100ms (in two way travel time).

The main rock components of this delta system are sand and shale, and the porosity ranges from 20% to 33%. An abundance of interesting zones can be seen in the sigmoidal bedding. The most striking feature is the high seismic amplitudes in the low-stand system tract, is shown in Figure 2.1.

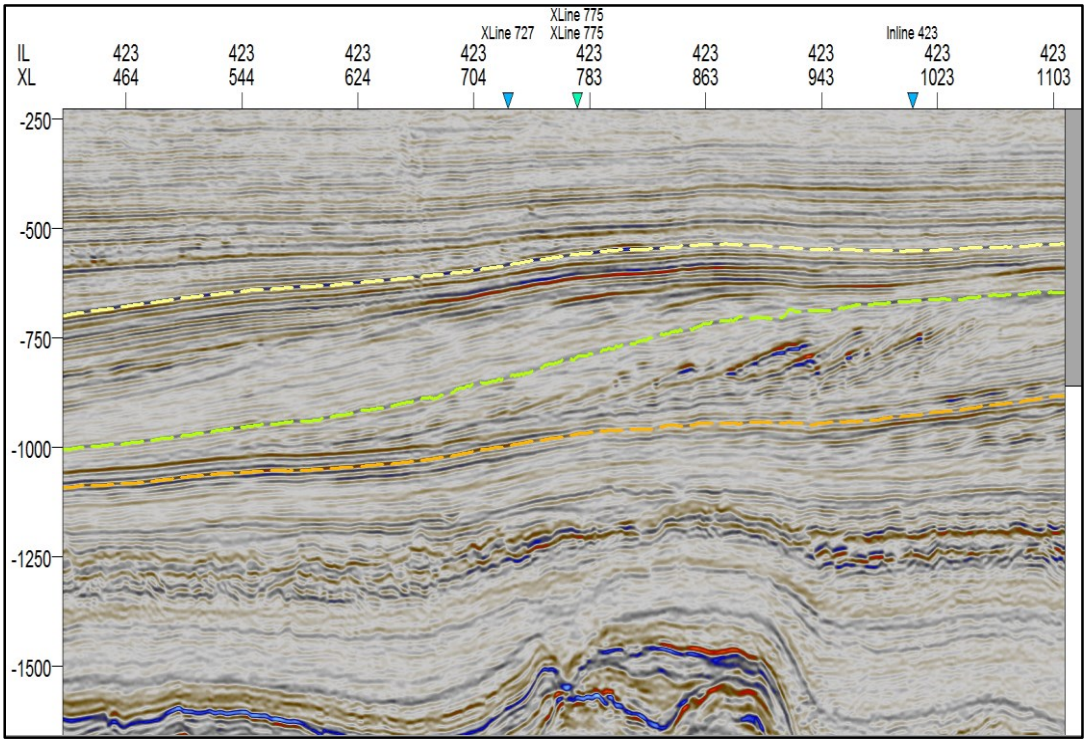

Figure 2.2. Large scale sigmoidal bedding in F3-block. The colored lines represent horizons tracked for inversion and used in this study.

3. **Methods**

Porosity is an important property of potential reservoirs. In order to predict the porosity away from the borehole, we need to calculate the impedance model throughout the entire seismic volume. Then, we can construct the relationship between the impedance and porosity from the well log data and use this relationship to convert the impedance inversion model to porosity model.

We applied the deterministic and stochastic inversion of post-stack seismic data for the estimation of acoustic impedance, and ultimately the porosity, in the target zone. The basic workflow is shown in the Figure 3.1.

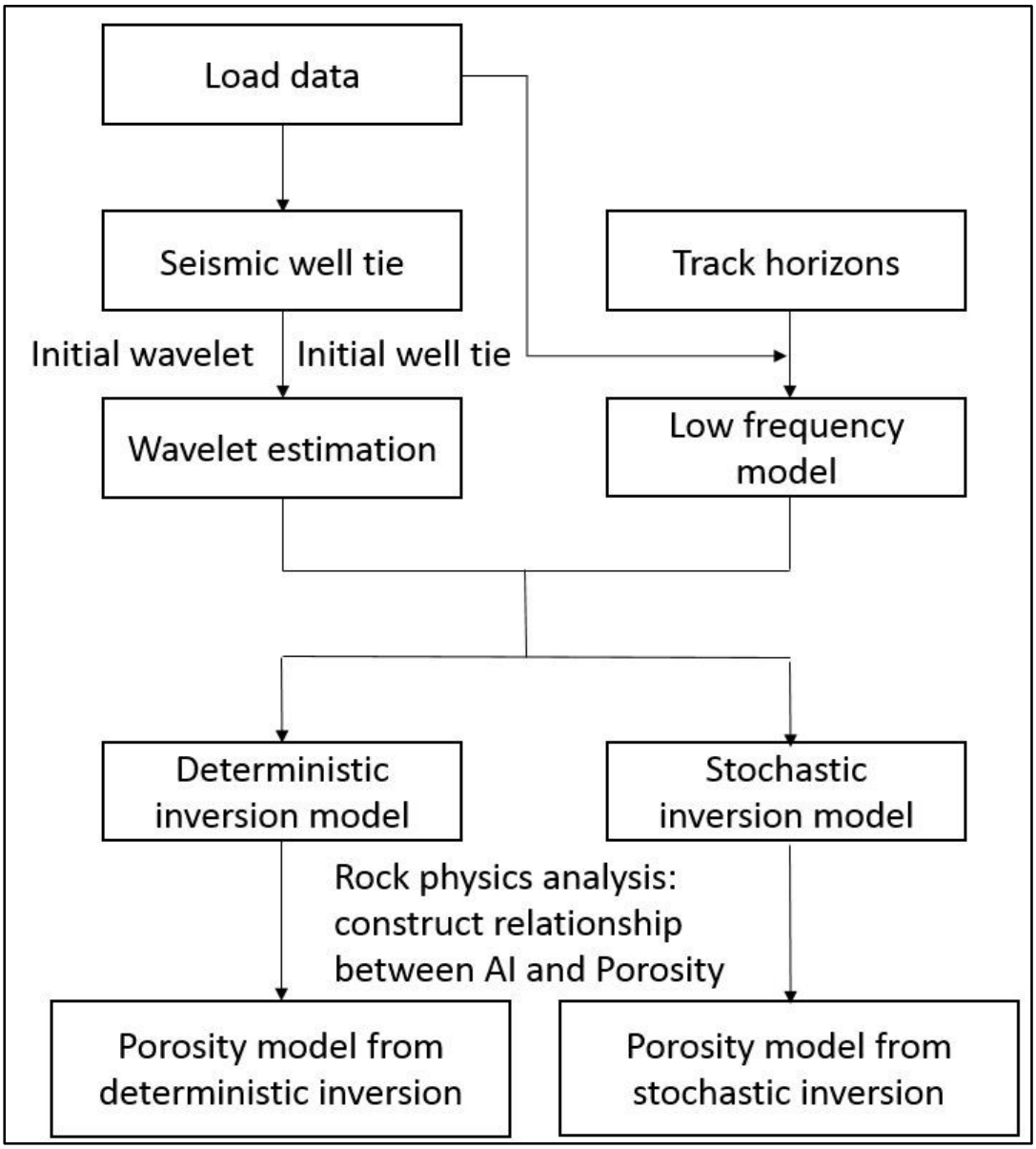

Figure 3.1. Basic workflow.

3.1. Initial seismic well tie

Tying wells to seismic information is a key step to relate the respective data between time and depth domains. This process includes building a time-depth relationship by first combining the sonic velocity and bulk density to create an initial synthetic trace, then applying a bulk shift, and then stretching or squeezing to make the synthetic trace match the input seismic trace near the well.

Because there are no check-shot data in this area, we used the density log and sonic log convolved with a Ricker wavelet to create the synthetic seismogram to obtain an initial well tie (Peterson, 1955). The initial well-ties and wavelets for each well are shown in the following figures.

From this step, the time-depth relationship is used in the following wavelet estimation. The parameters of initial wavelet that we obtained are:

- Wavelet type: Ricker wavelet.
- Main frequency: 45 Hz.
- Phase: 180 degree phase shift.
- Length: 120ms.

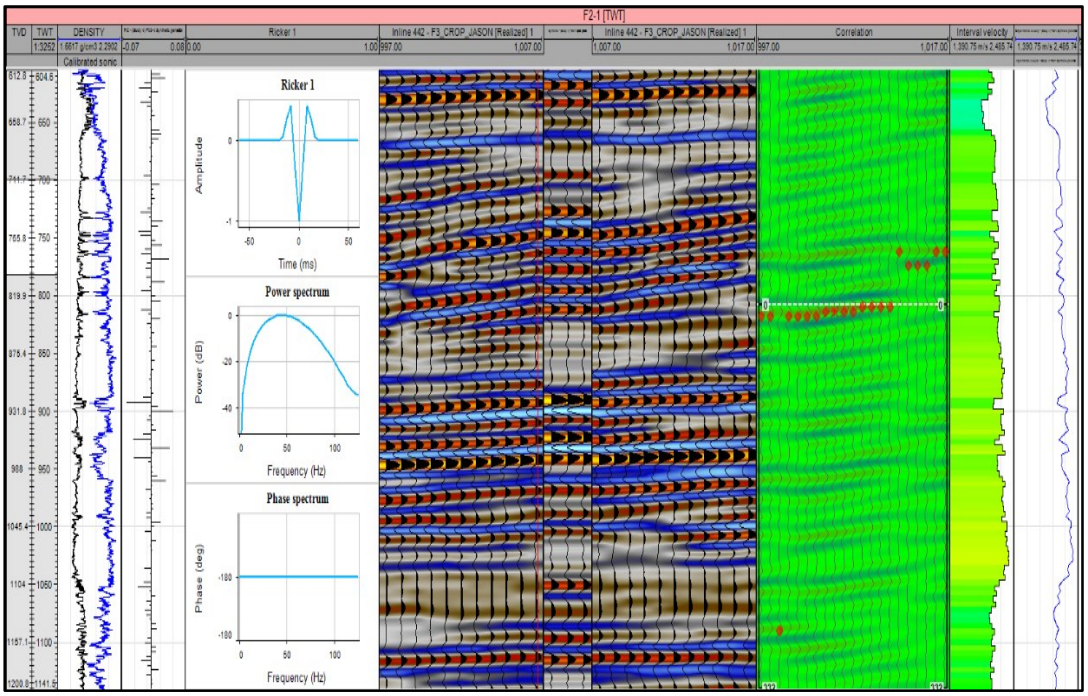

Figure 3.2. Initial seismic well tie of well F2-1.

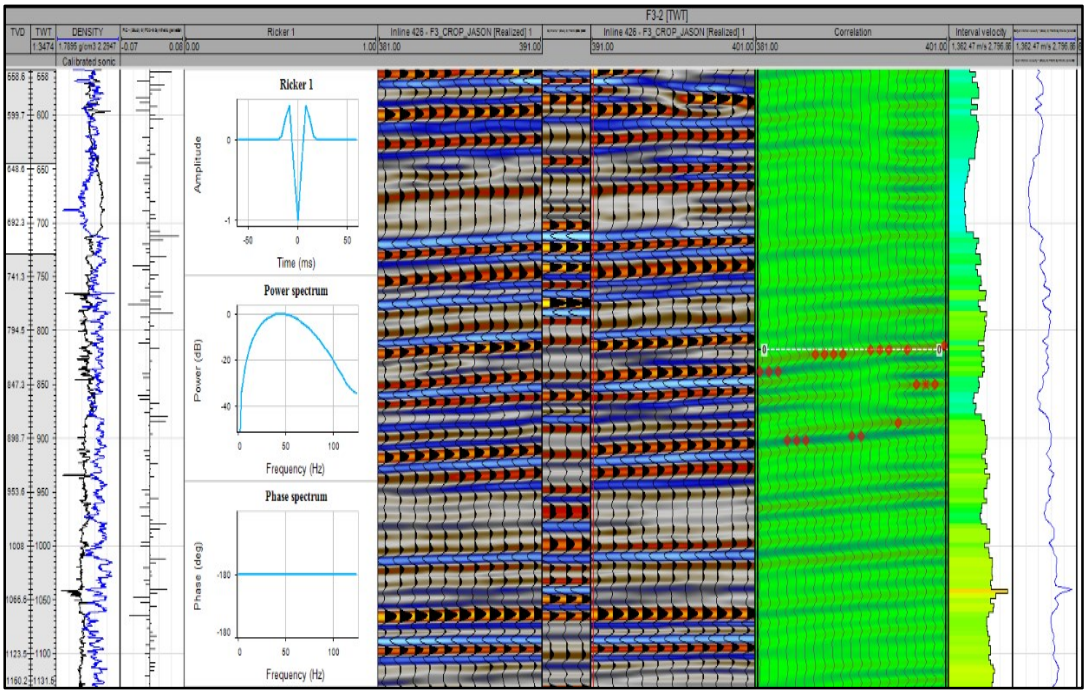

Figure 3.3. Initial seismic well tie of well F3-2.

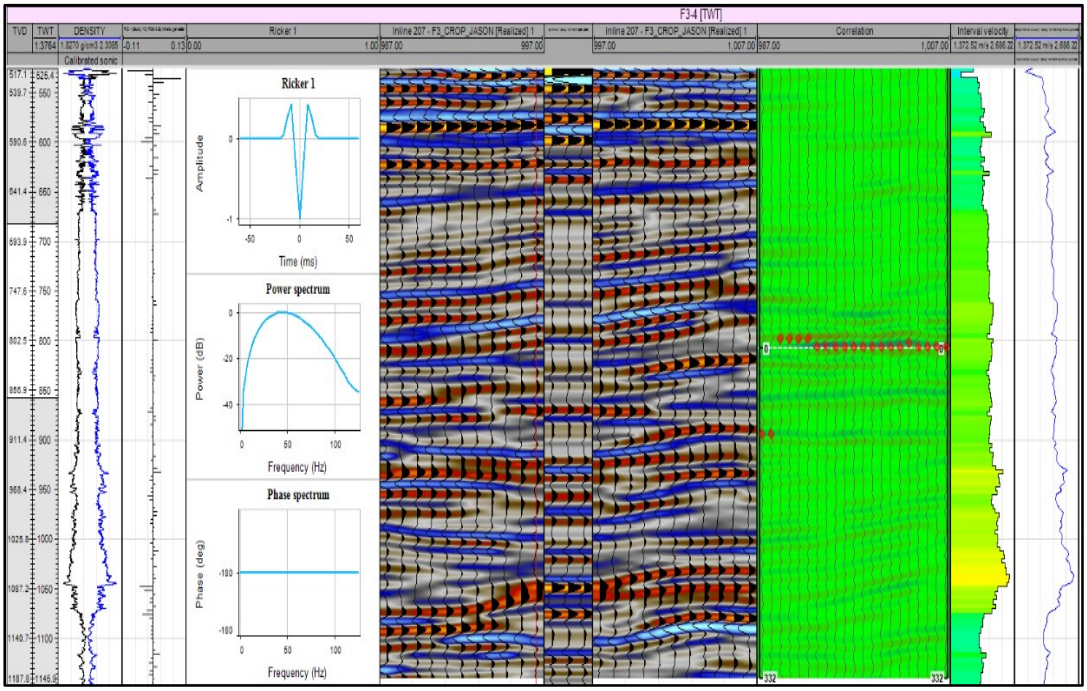

Figure 3.4. Initial seismic well tie of well F3-4.

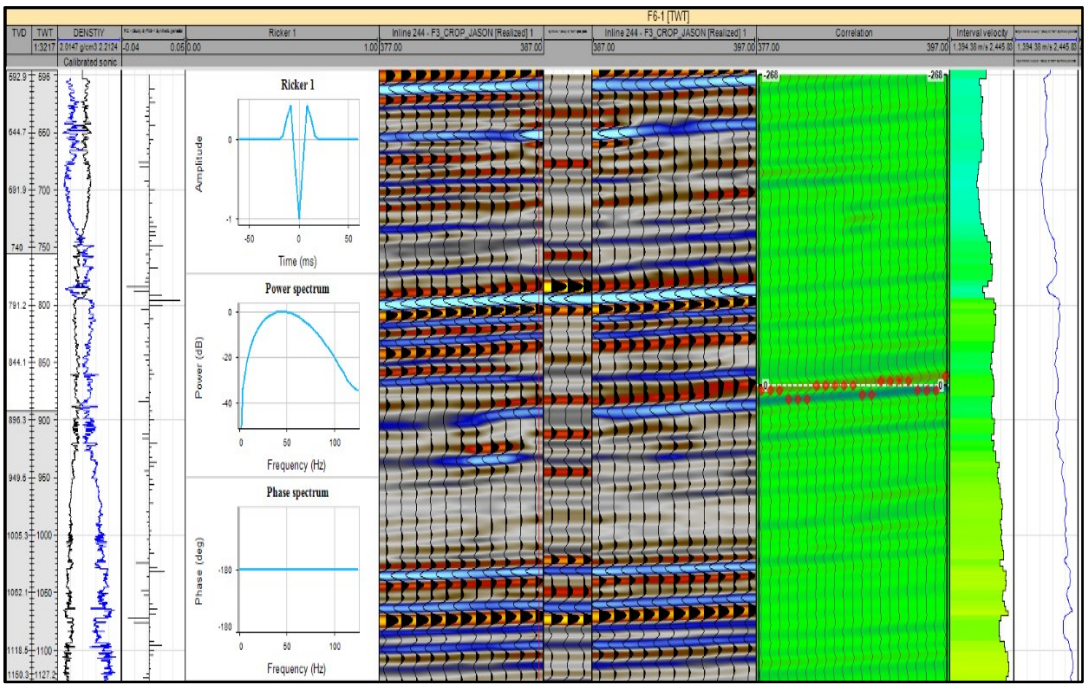

Figure 3.5. Initial seismic well tie of well F6-1.

3.2. Wavelet estimation

The various methods of seismic inversion require more accurately estimating a wavelet from the data than the initial well-tie, because the source wavelet is not necessarily the same at different locations, and the wavelet propagated in the subsurface is complicated by various effects. The final wavelet represented in the data is rarely as simple as the conventional Ricker model. To obtain a good wavelet is one of the most important and most time consuming parts, and it can affect whether the final inversion model is reliable or not.

In order to extract a reliable wavelet, incorporation with wells is necessary.

3.2.1. Well tie

Building an adequate tie between the seismic data and the well is a critical step for the wavelet estimation (all the examples in the following figures are shown for the well F06-1).

The workflow has five steps:

I. Load the acoustic impedance (product of sonic velocity and bulk density) in depth domain.

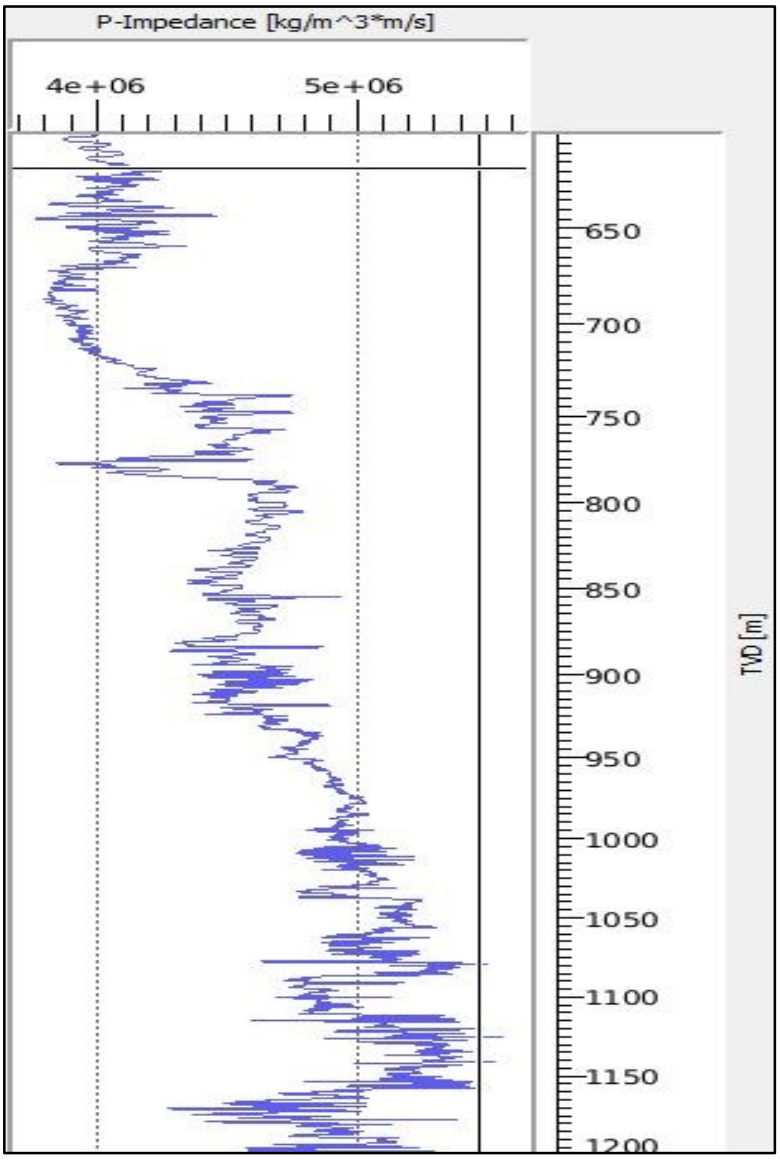

Figure 3.6. Acoustic impedance log in depth domain.

II. Load an initial time-depth relationship from the velocity data, resembling check-shot survey. Convert the impedance log from depth phase into time phase.

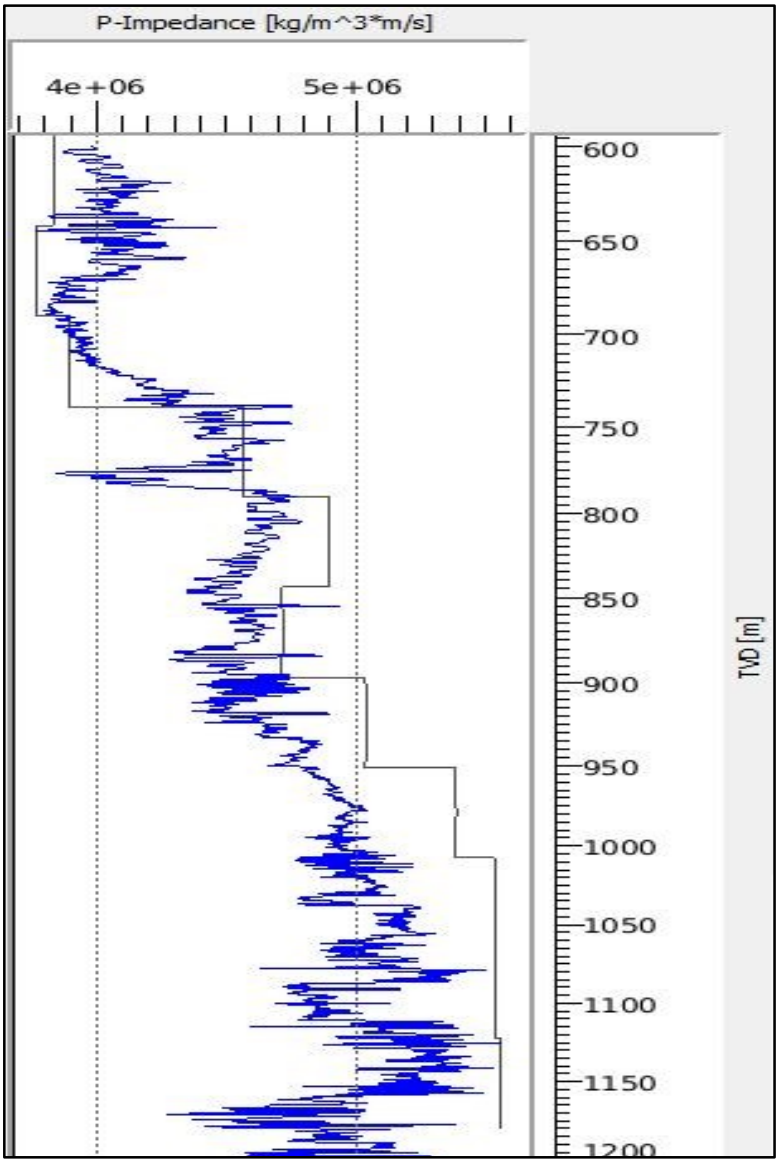

Figure 3.7. Initial time-depth relationship.

III. Create a synthetic wavelet. Often, a Ricker wavelet with frequency content similar to that of the seismic data is good enough as an initial wavelet.

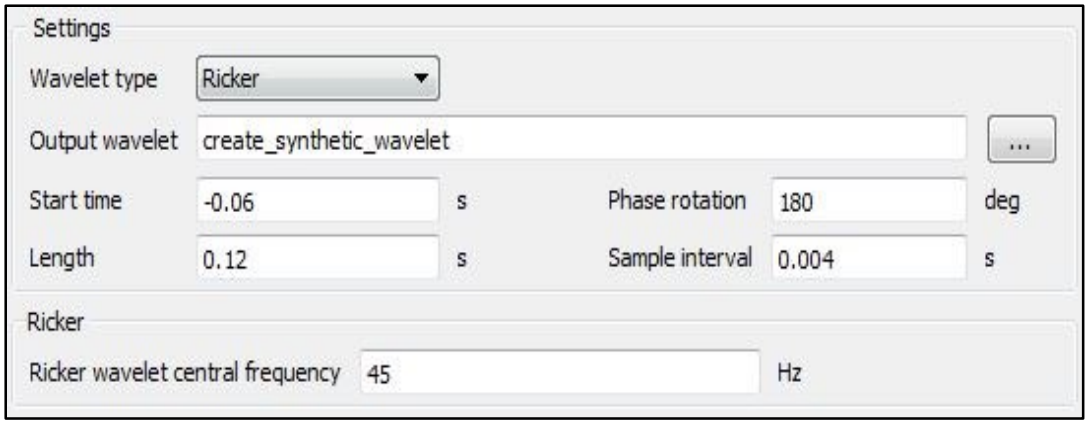

Figure 3.8. Parameters of initial wavelet.

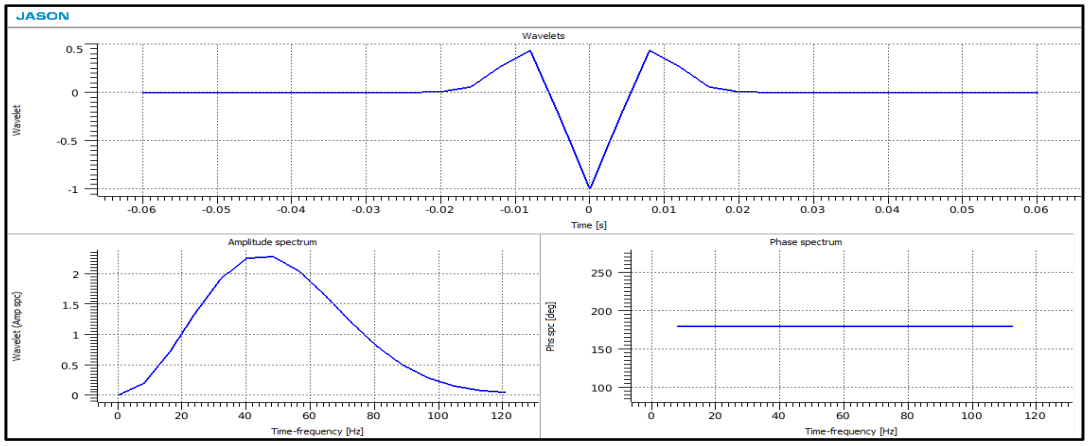

Figure 3.9. Created synthetic wavelet.

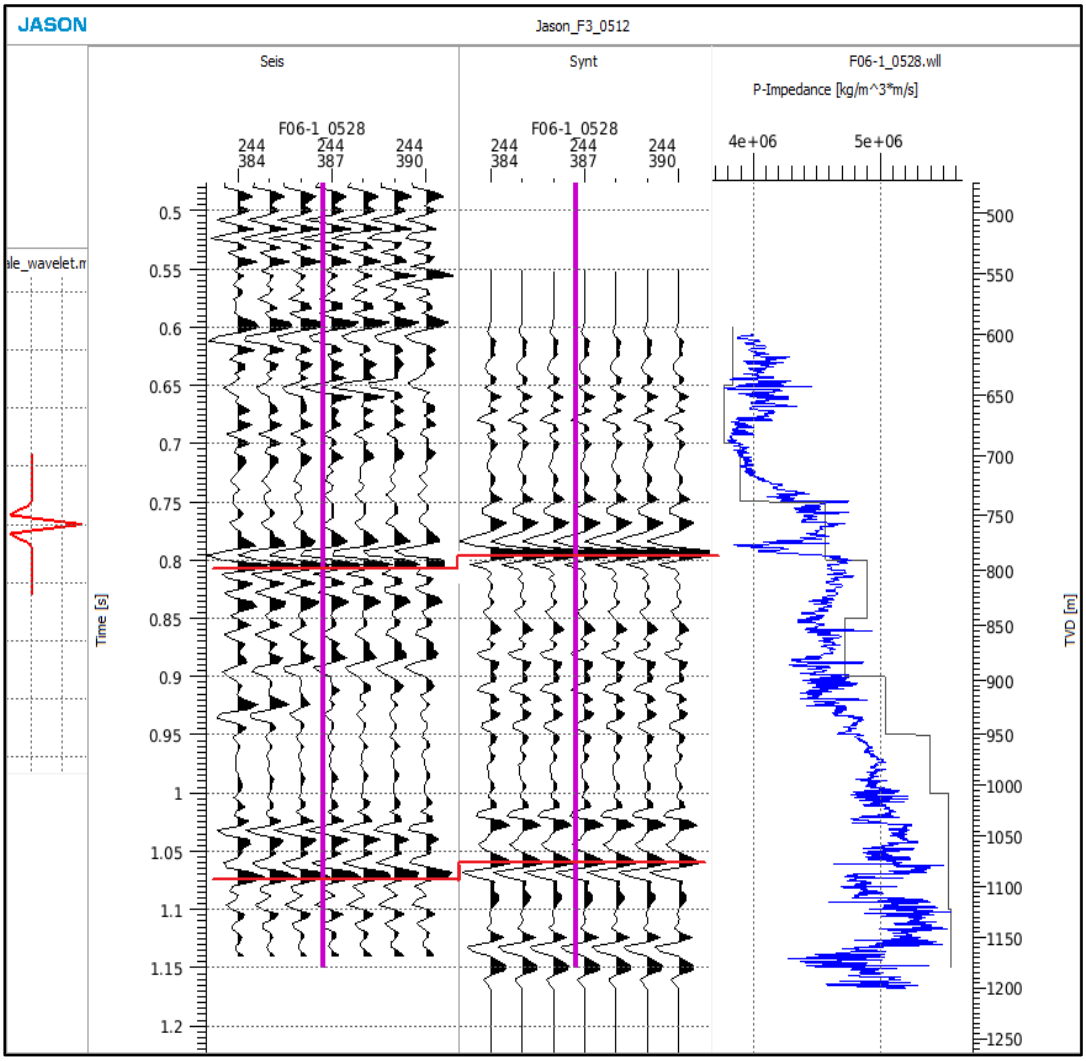

Figure 3.10. Initial synthetic seismogram. The seismic data is in the first panel and the initial synthetic seismogram in the second panel. The main events do not match.

IV. Bulk shift the synthetic seismogram to make the peaks of the main events line up with the seismic data, then stretch and squeeze sections to fit other events.

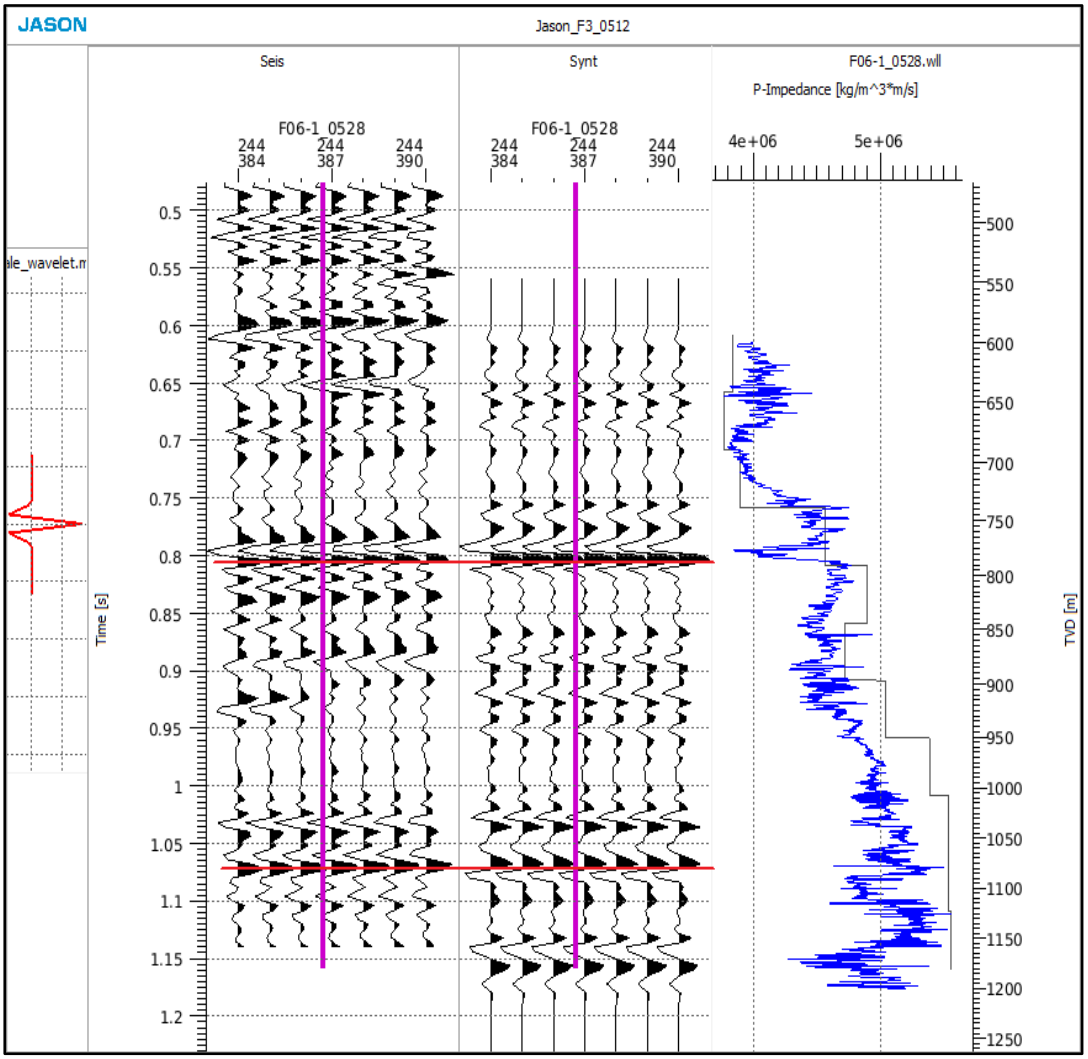

Figure 3.11. Make the main events of synthetic seismogram line up with the seismic data.

V. Quality control the stretch and squeeze. During the stretch and squeeze, over-tie is often encountered. In that case, we compare the relative difference between the time log of the sonic log after stretch or squeeze and the time log from the original sonic log (Figure 3.10.). When applying the stretch and squeeze, the difference should be constrained in an acceptable.

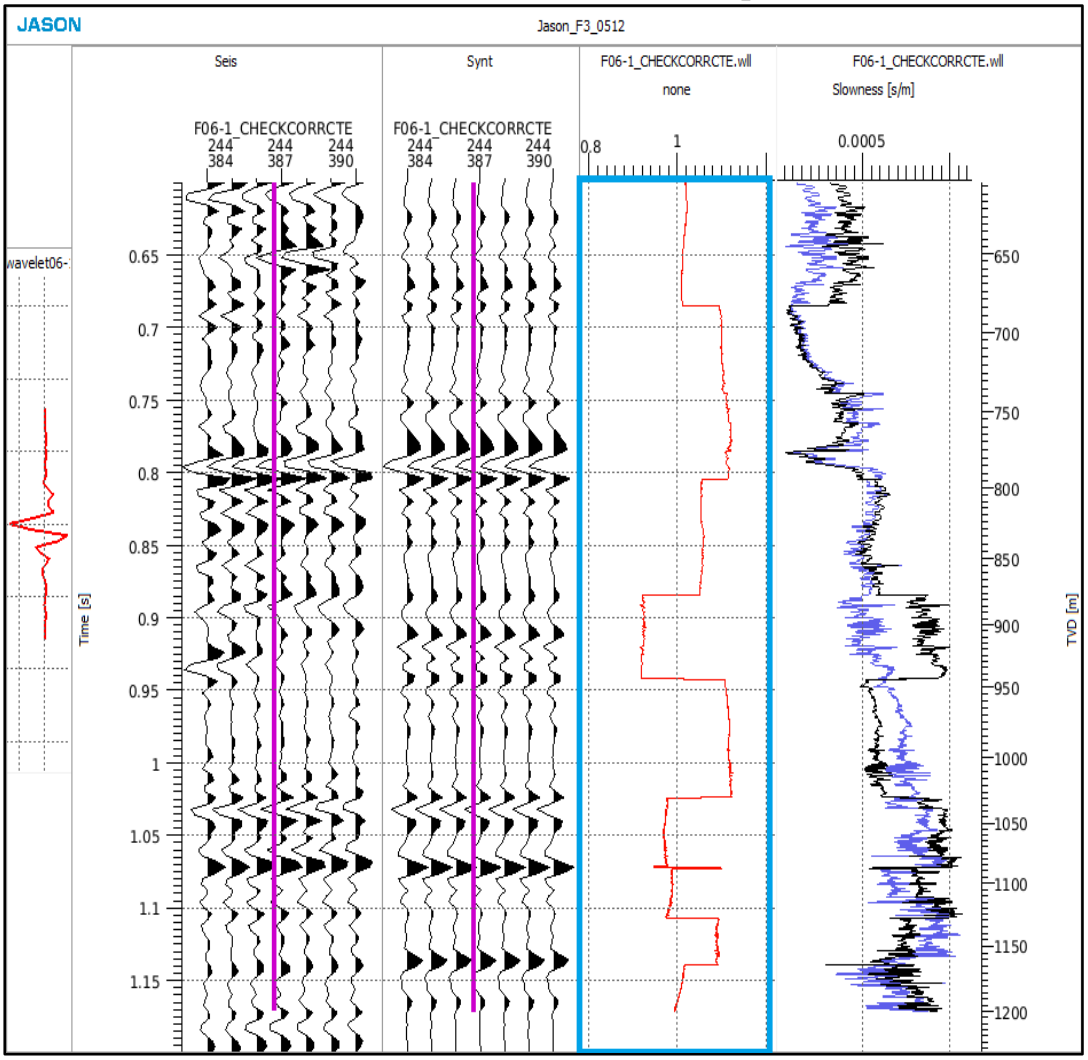

Figure 3.12. Quality control the stretch and squeeze. The red line in the blue box represent the relative difference between the time log based on the sonic log after stretching or squeezing and the original sonic log.

3.2.2. Extract wavelet

We will extract a wavelet after achieved a reasonable seismic well tie. This procedure will be conducted at each well individually and we extract the wavelet per well. There were only two wells that had density logs. At the other wells, pseudo-logs for density were used, having been created by OpendTect from gamma-ray and sonic logs using a neural-network approach (dGB Earth Sciences).

The following show the seismic well tie for each well and estimated wavelet from the well F6-1 (the correlation is 0.77), the highest correlation of wavelets that obtained from other three wells is 0.51, 0.46 and 0.48, respectively. So we just used the wavelet that we extracted from the well F6-1 in the inversion instead of using the average of the four wavelets.

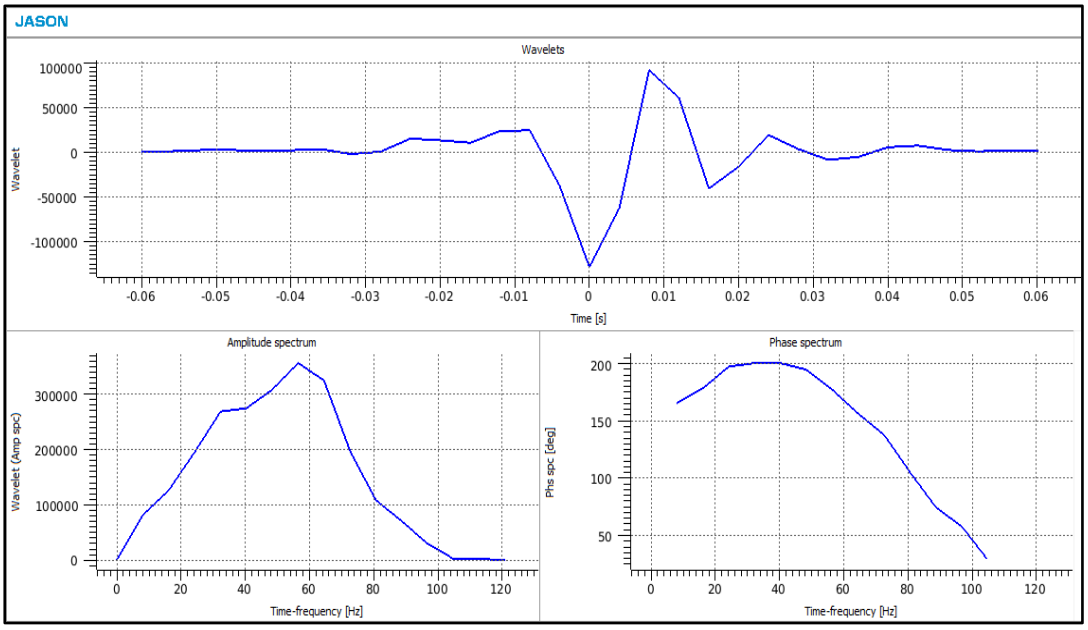

Figure 3.13. The final wavelet used in the inversion.

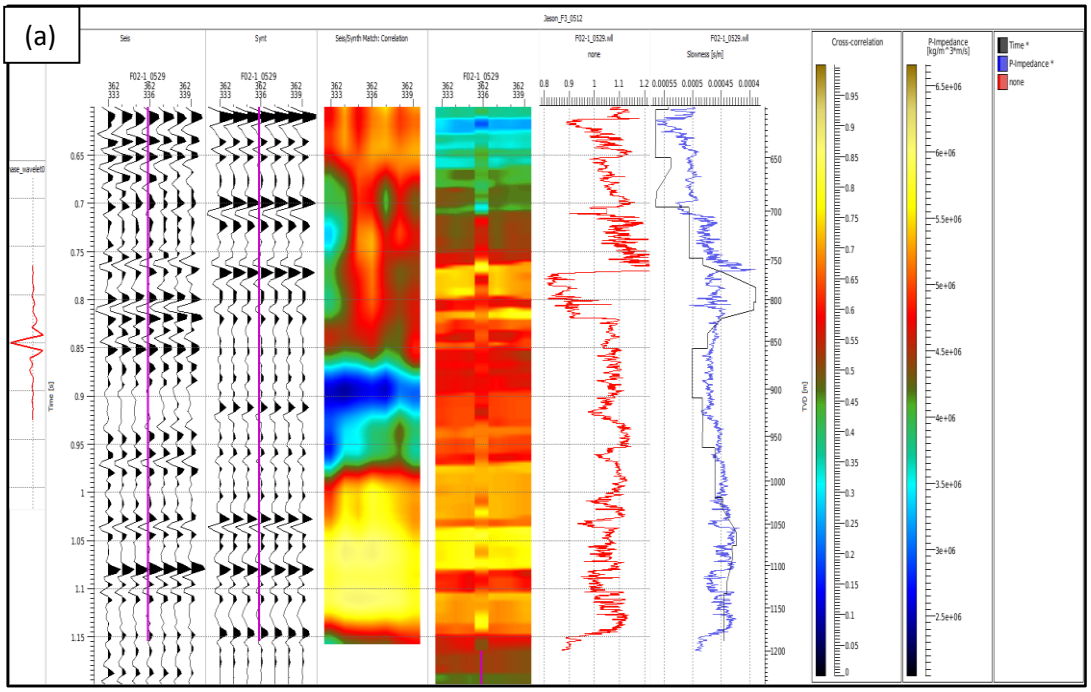
(a)
Seis
Synt
Seis/Synth Match: Correlation
F02-1_0529
Cross-correlation
P-Impedance [kg/m^3*m/s]
Time *
P-Impedance *
none
Time [s]
TVD [m]

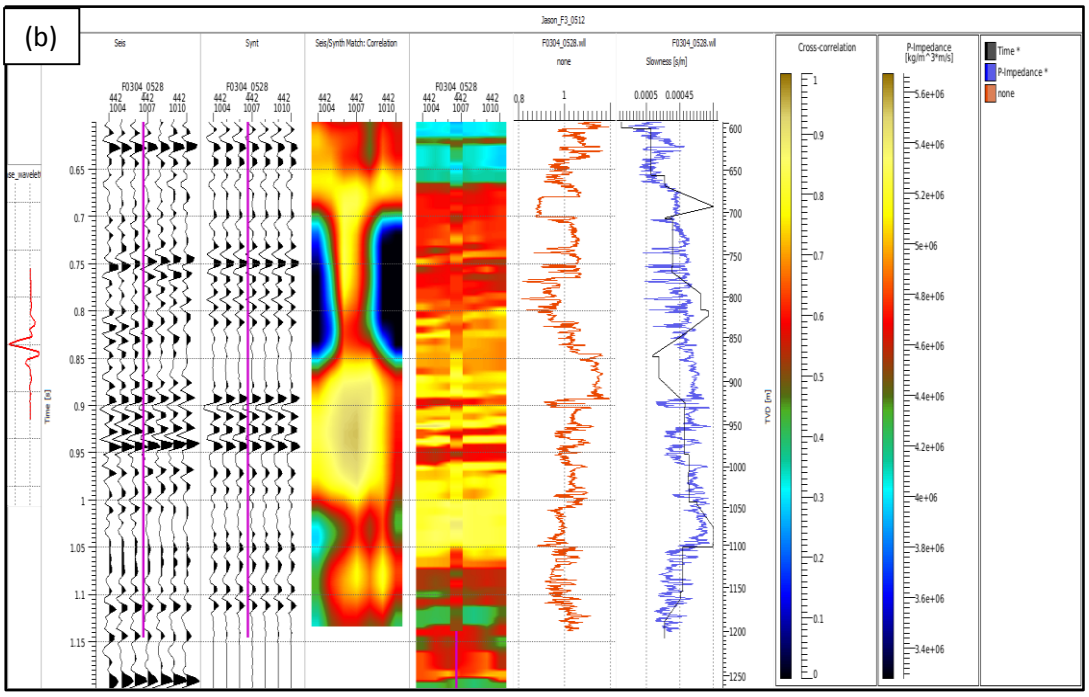
(b)
Jason_F3_0512
Seis
Synt
Seis/Synth Match: Correlation
F0304_0528.wll
none
F0304_0528.wll
Slowness [s/m]
Cross-correlation
P-Impedance [kg/m^3*m/s]
Time *
P-Impedance *
none
F0304_0528
442
1004
1007
1010
0.8
1
0.0005
0.00045
Time [s]
TVD [m]

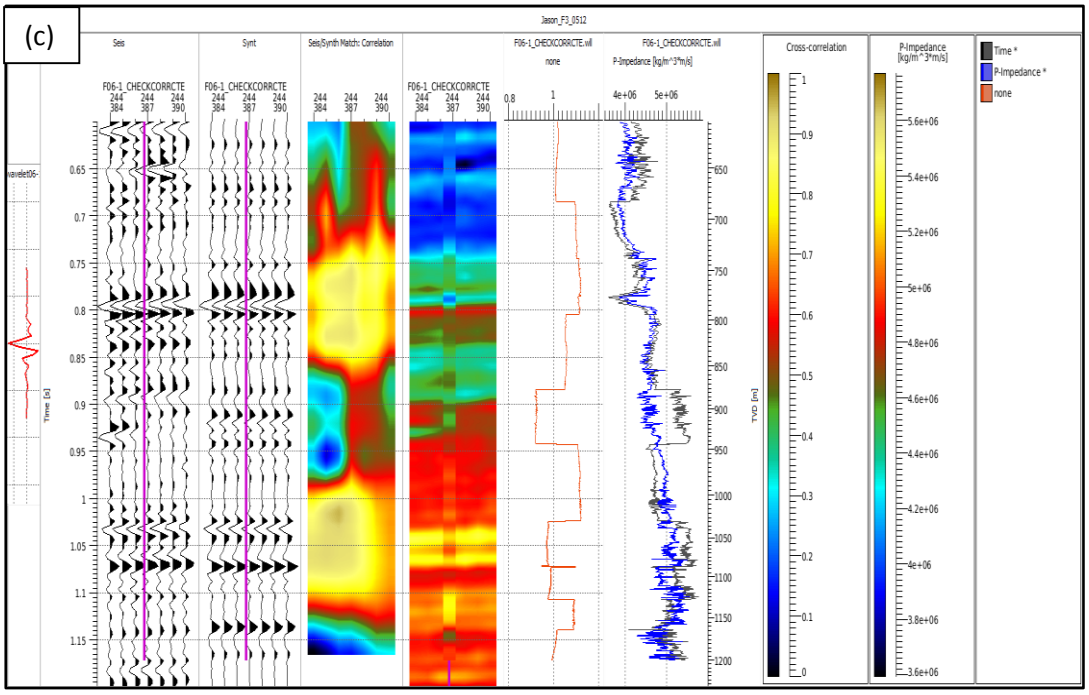
(c)
Jason_F3_0512
Seis
Synt
Seis/Synth Match: Correlation
F06-1_CHECKCORRCTE.wll
none
F06-1_CHECKCORRCTE.wll
P-Impedance [kg/m^3*m/s]
Cross-correlation
P-Impedance [kg/m^3*m/s]
Time *
P-Impedance *
none
Time [s]
TVD [m]

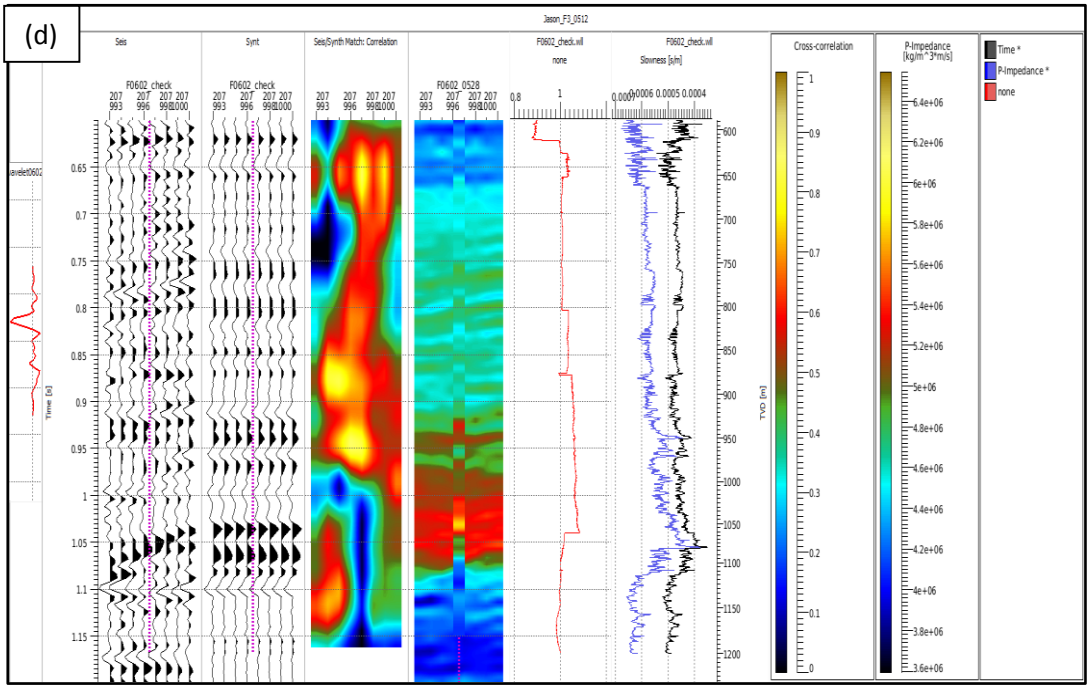

Figure 3.14. Final Seismic well tie and estimated wavelet of the four wells (a) Final seismic well tie for F2-1. (b) Final seismic well tie for F3-2. (c) Final seismic well tie for F3-4. (d) Final seismic well tie for F6-1. Within each figure, the panels, from left to right, contain: the wavelet; the actual seismic data near the well; the synthetic seismogram; the correlation between the synthetic seismogram and the seismic data near the well; the impedance log and the inversion result which combine the wavelet with the seismic trace near the well; Relative difference between the time log from the sonic log after stretching and squeezing and the time log from the original sonic log; the impedance curve and initial time-depth relationship.

3.3. Low frequency model

In our case, we do not have pre-stack data and cannot perform a velocity analysis in this volume. Here we constructed a 3D broadband impedance model of the sub-subsurface by using well-log data and picked seismic horizons to guide the interpolation between wells.

In order to estimate the variation trend of the impedance at the non-well area for the following stochastic inversion, a variogram analysis is necessary (Stefan, 1999). Because the variation trend of impedance is constrained by 3D anisotropic variogram. The horizontal and vertical variogram analysis from this survey is shown in the Figures 3.15-3.18. After variogram analyses and interpolating the wells, a low frequency model is obtained shown in Figure3.19.

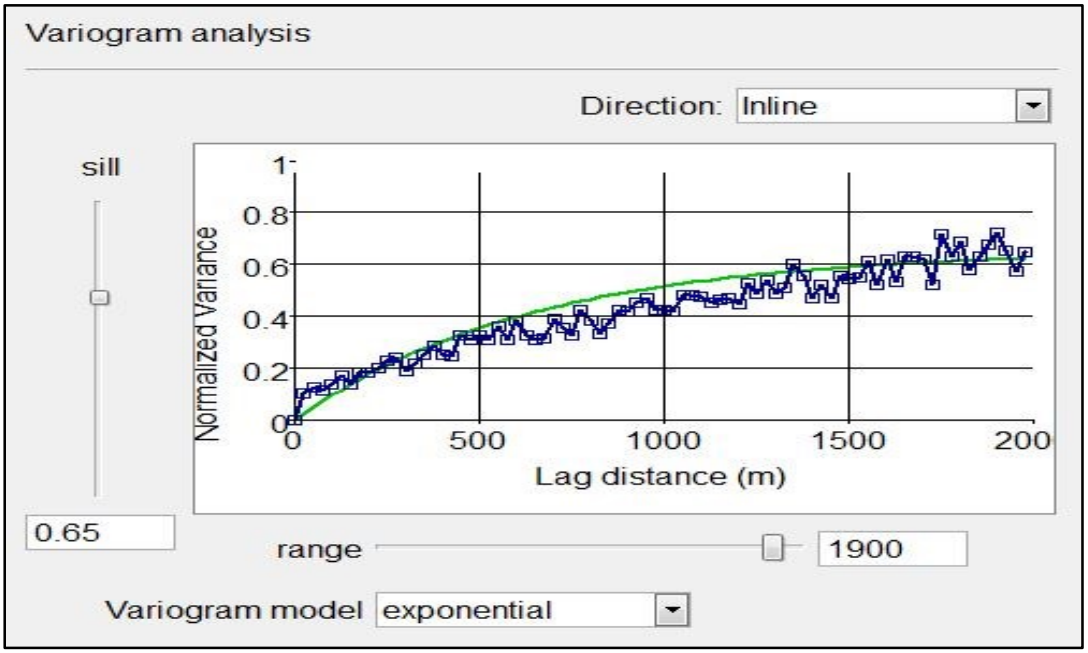

Figure 3.15. Horizontal variogram analysis along the inline direction.

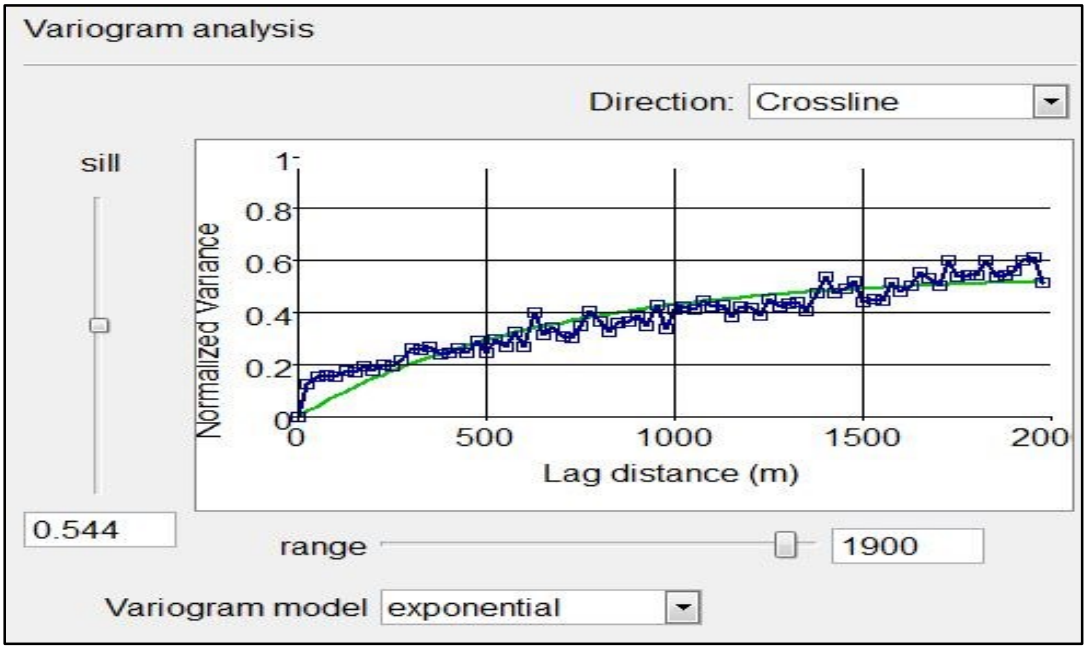

Figure 3.16. Horizontal variogram analysis along the crossline direction.

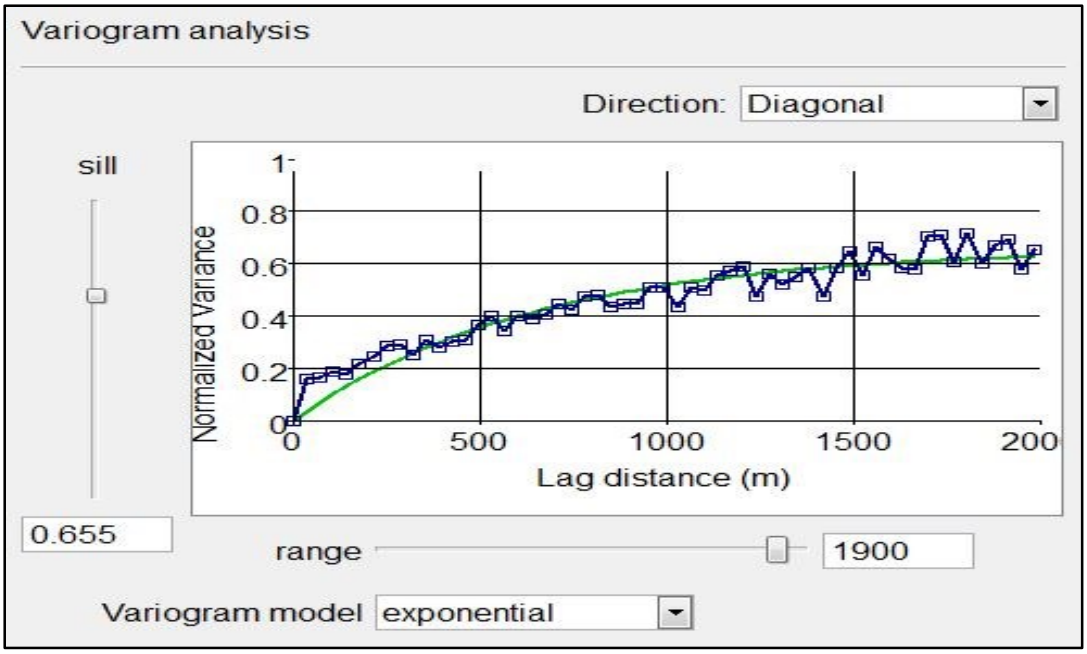

Figure 3.17. Horizontal variogram analysis in a diagonal direction.

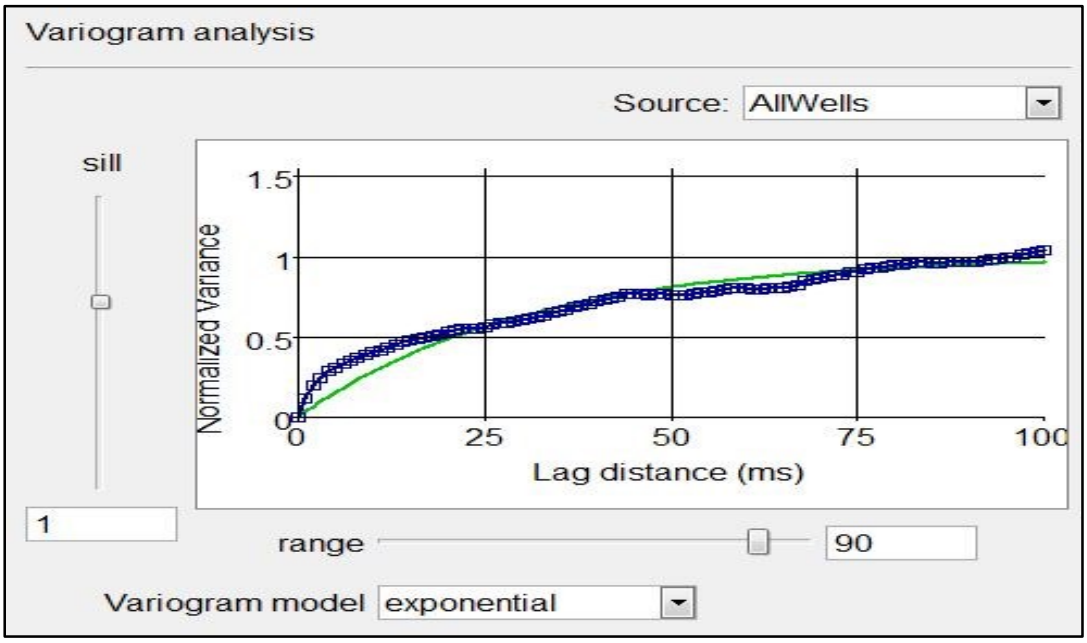

Figure 3.18. Vertical (in time) variogram analysis.

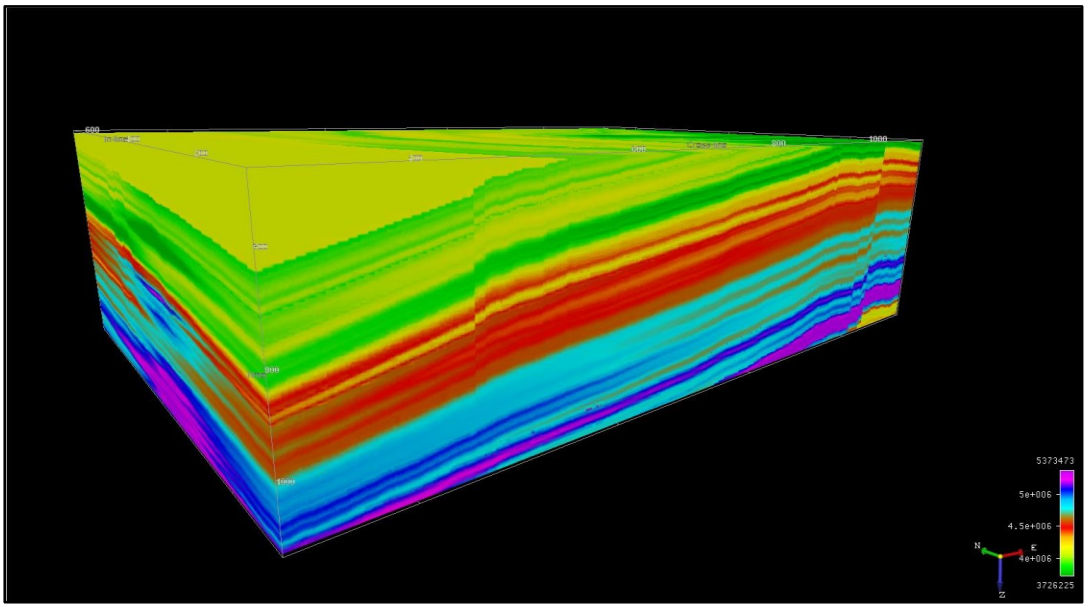

Figure 3.19. Low frequency model.

3.4. Inversion

3.4.1. Deterministic inversion

The deterministic inversion method used in this study is model-based and uses a broad-band impedance as the initial model. The inversion starts by evaluating the error between the synthetic trace and the input seismic trace. If the error between these two terms is not small enough, the algorithm will update the synthetic trace and put it into the next iteration and keep this process until the error meets the exit threshold (Barclay, 2008).

In this study, a deterministic inversion model which represent the absolute impedance is shown in the Figure 3.20.

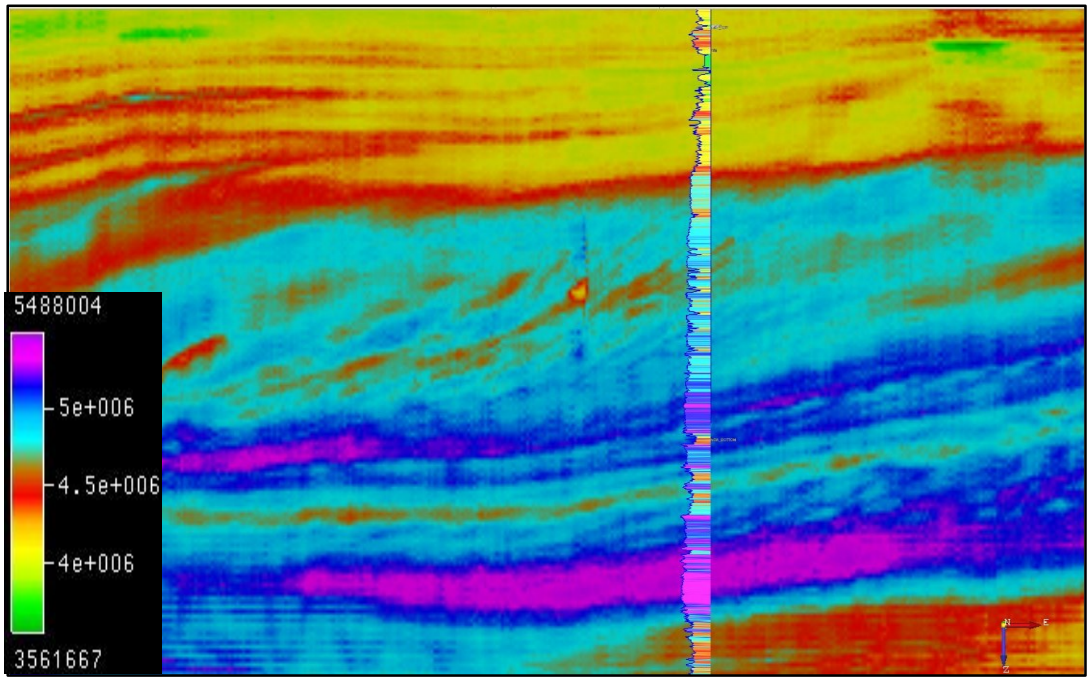

Figure 3.20. Absolute acoustic impedance model from deterministic inversion.

3.4.2. Blind well test for deterministic inversion

As the seismic inversion is processing over a large 3D data sets, it is important and necessary to understand what is going to be achievable and whether the inversion result is reliable. In order to check the result of the inversion model is valid or not, we applied the blind well test to investigate the result (Hasanusi, 2007).

Since there are four wells in this area, we first choose three wells (in random) into the inversion model calculation and leave one well as “blind well”. Then compare the impedance log from the blind well and the impedance inversion result near the blind well location.

The blind well test for the deterministic inversion model is shown in the Figure 3.21. Most of the impedance log can match the inversion result near the well and confirms that the inversion model can be used in the non-well area.

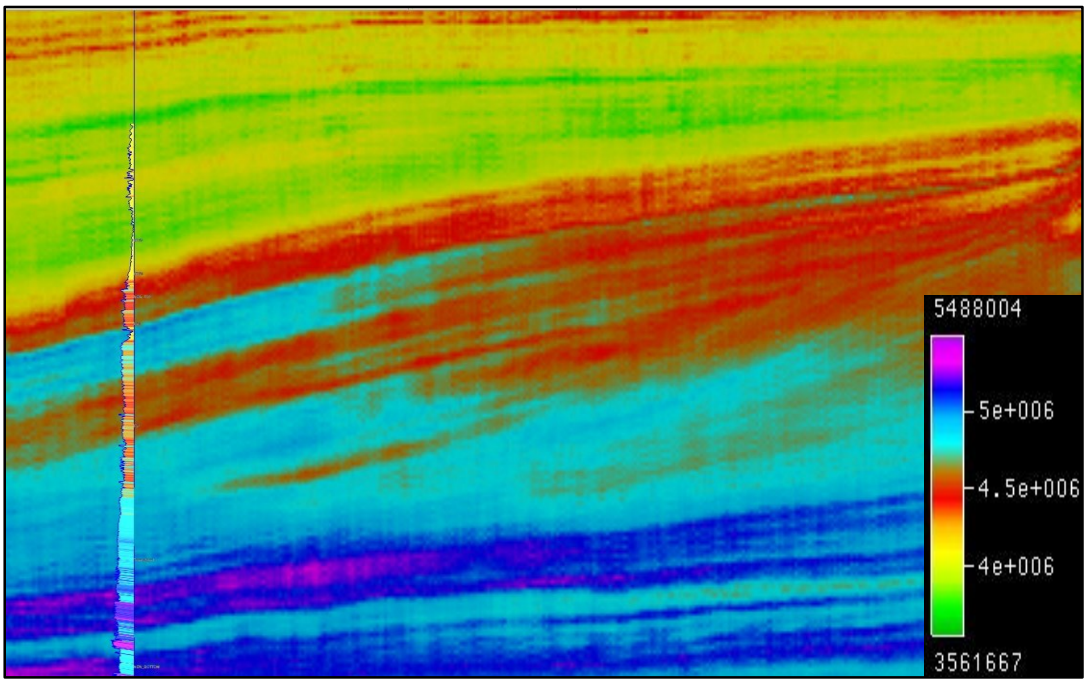

Figure 3.21. Blind well test for deterministic inversion model.

3.4.3. Stochastic inversion

The basis of the stochastic inversion is geo-statistical (Verma et al, 2014). A variogram analysis is necessary before running the stochastic inversion to simulate the spatial variation at each direction. Since stochastic inversion is non-uniqueness, a large number of realizations would be generated during the inversion. Each realization is the same at the well locations, but the inversion results are increasingly different further away from the well. The final stochastic inversion model that is used in this study to predict the porosity is the average of all twenty realizations obtained.

The initial impedance model used in this article was constructed based on the picked horizons and wells, and apply it into the stochastic inversion. In this project, we simulated 20 realizations of absolute acoustic impedance. There are three different realizations of acoustic impedance shown in the Figure 3.22.

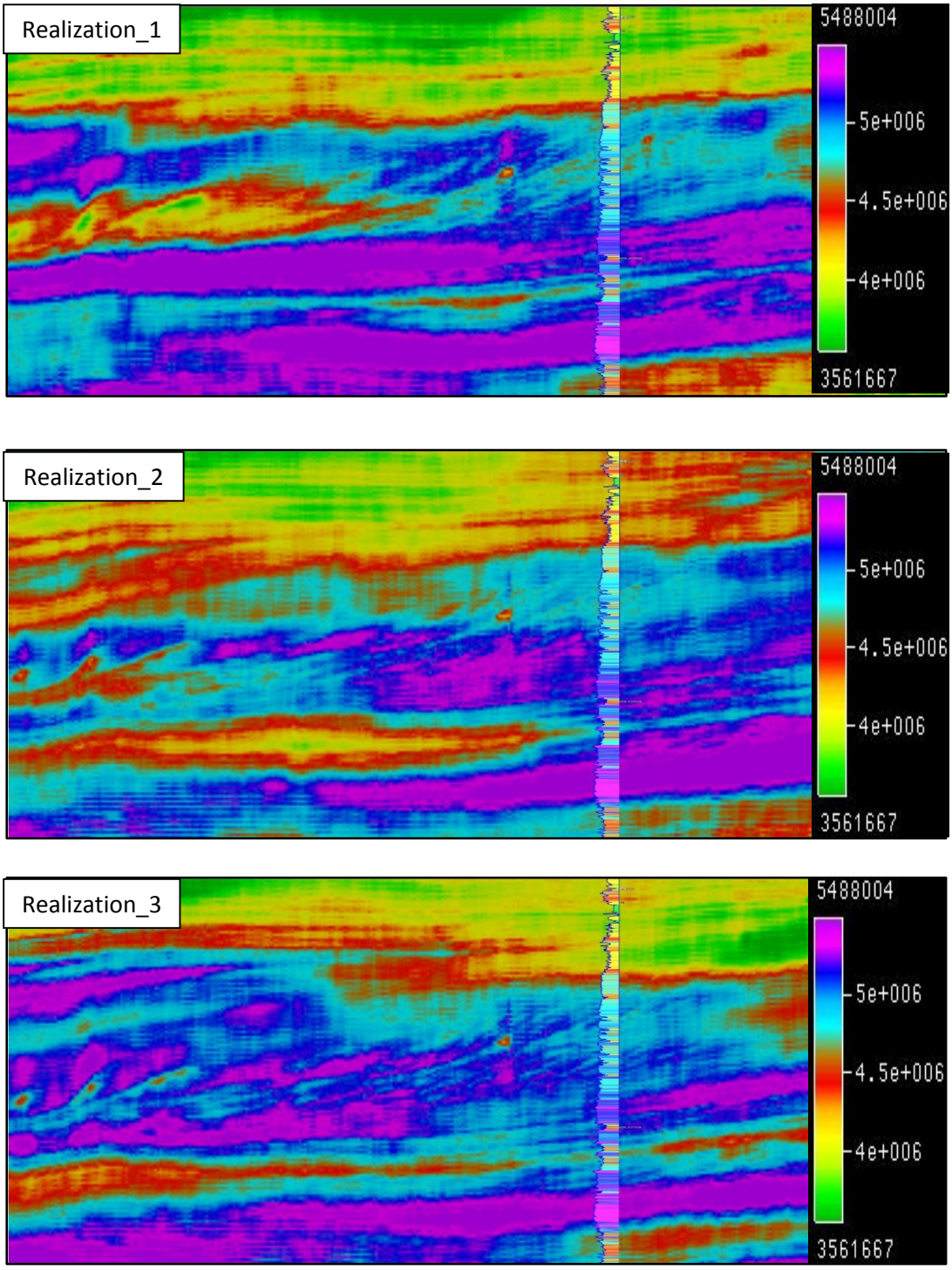

Figure 3.22. Three different realizations of the 20 different realizations from stochastic inversion.

3.4.4. Blind well test for stochastic inversion

As with the deterministic inversion, the stochastic inversion also needs to apply the blind well test to check the reliability of the inversion result. The inversion model that is used for this check is the mean of all the 20 realizations. From Figure 3.23. the impedance log of the blind well and the mean of realizations at the blind well location can be seen to match each other well.

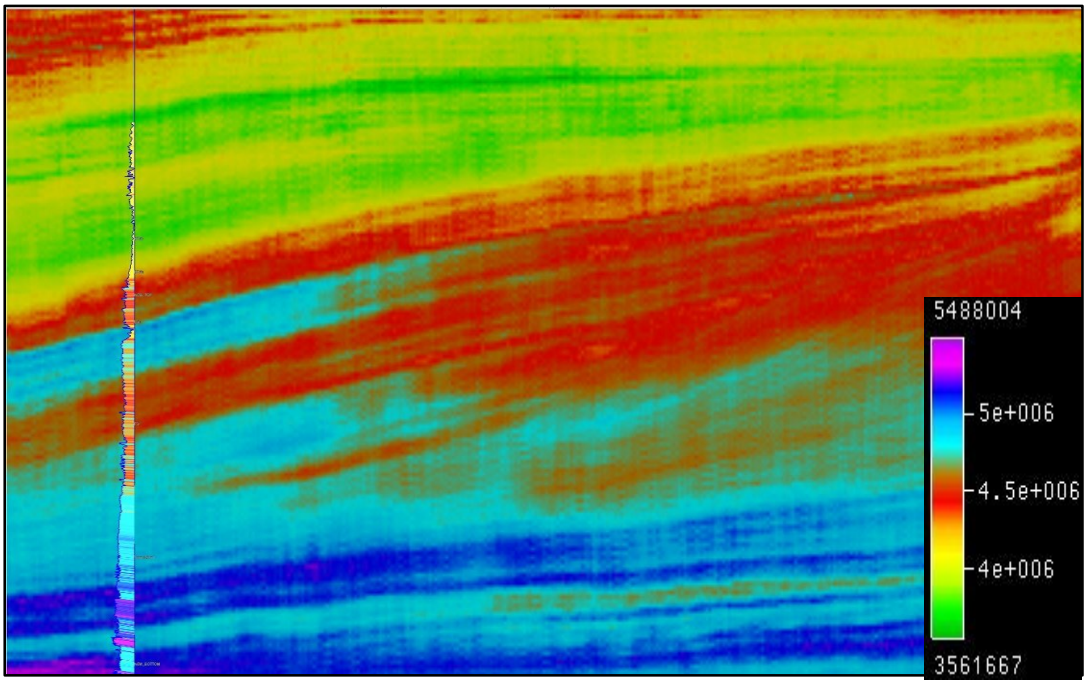

Figure 3.23. Blind well test for stochastic inversion.

3.5. Rock physics analysis

3.5.1. Density – Velocity

Velocity is correlated with density in the subsurface and there are empirical relationships between this two properties for shales, sandstones and carbonate. Here we use: $\rho = aV^m$ (Gardner et al, 1974).

In the Gardner equation, ρ is density, V is velocity, a and m are a coefficient and exponent, respectively, to be determined through calibration. For different lithologies or saturations, the a and m will not be constant.

In order to find the density-velocity relationship, we cross-plot the sonic (1/velocity) against the density log and colored by gamma ray for each well (Figure 3.24).

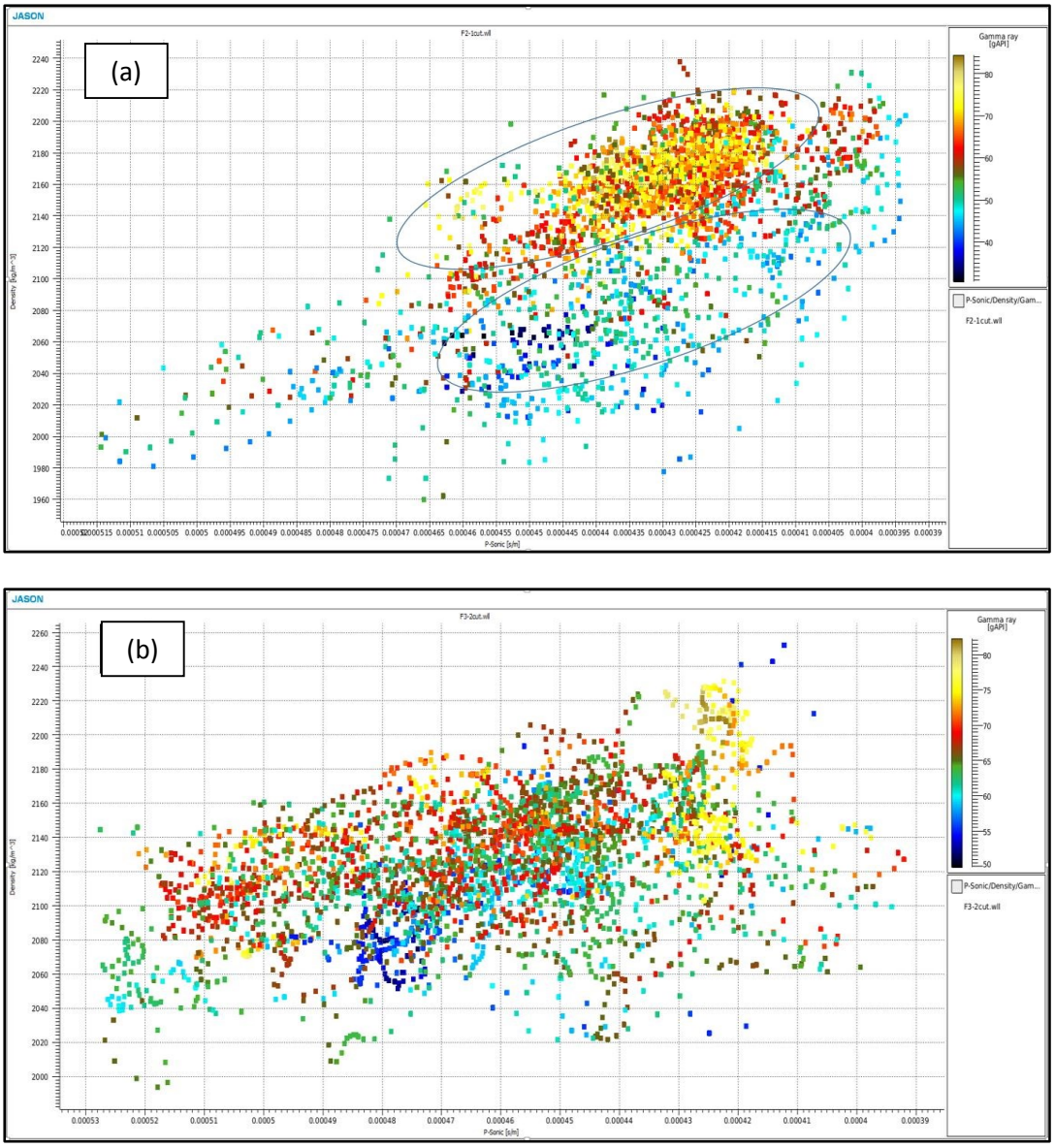

Figure 3.24. Cross plot of sonic and density colored by gamma ray (note: the color scales are not the same in the two plots). (a) Cross plot for the well F2-1, according to value of gamma ray we can separate those points into two parts. As gamma ray is the index for lithology, so in this well, we can find different relationship between different lithology. (b) Cross plot for the well F3-2. We cannot distinguish the lithology by gamma ray.

For well F2-1, we separate the data based on gamma ray, using 50 API as the cut off value, and we find the two relationships between density and velocity (Figure 3.25). Well F2-1 is in the more sand-prone low-stand tract, but also penetrates formations beneath this tract.

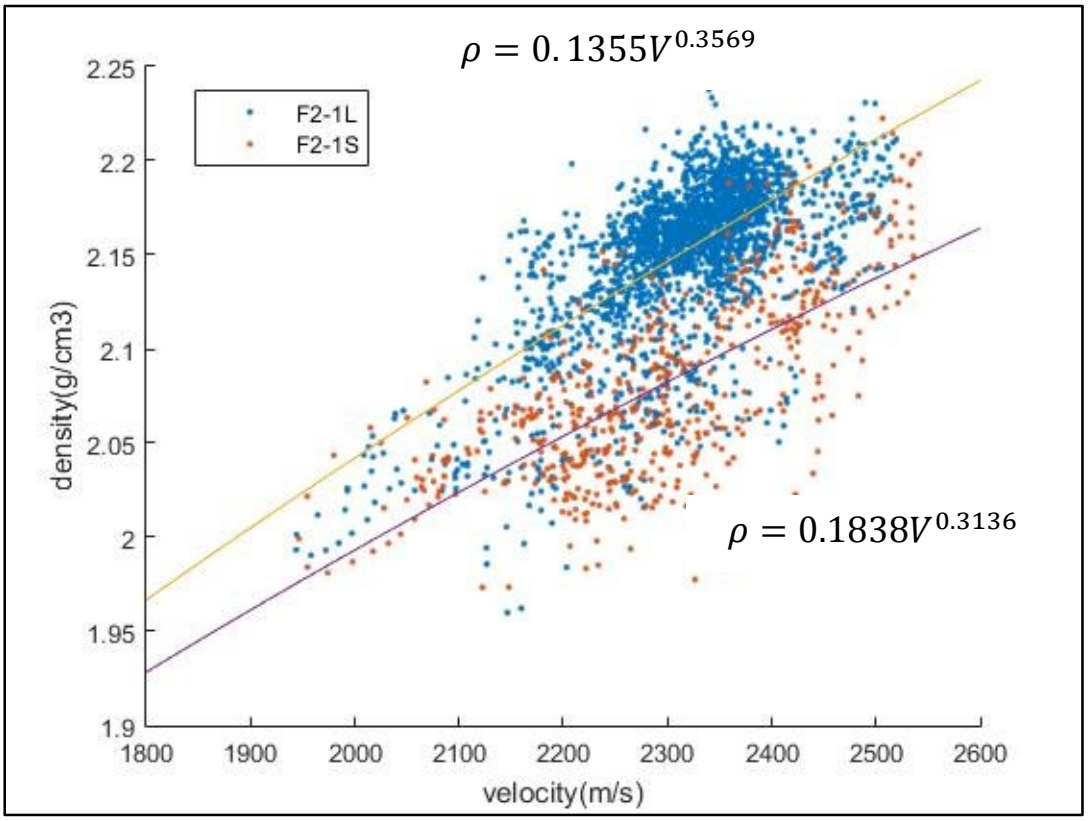

Figure 3.25. Cross plot of density and velocity and the Gardner relationship with different coefficient and exponent for well F2-1. The blue dots in the upper area represent gamma ray > 50 API, and the yellow line in that area represents their Gardner relationship of $\rho = 0.1355V^{0.3569}$. The orange dots and the purple line in the lower area represent gamma ray < 50 API with their Gardner relationship of $\rho = 0.1838V^{0.3136}$.

For the well F3-2, because all gamma ray values are greater than 50, we simply use all points to find one relationship between the density and velocity (Figure3.26). Well F3-2 is in the more shale-prone high-stand tract.

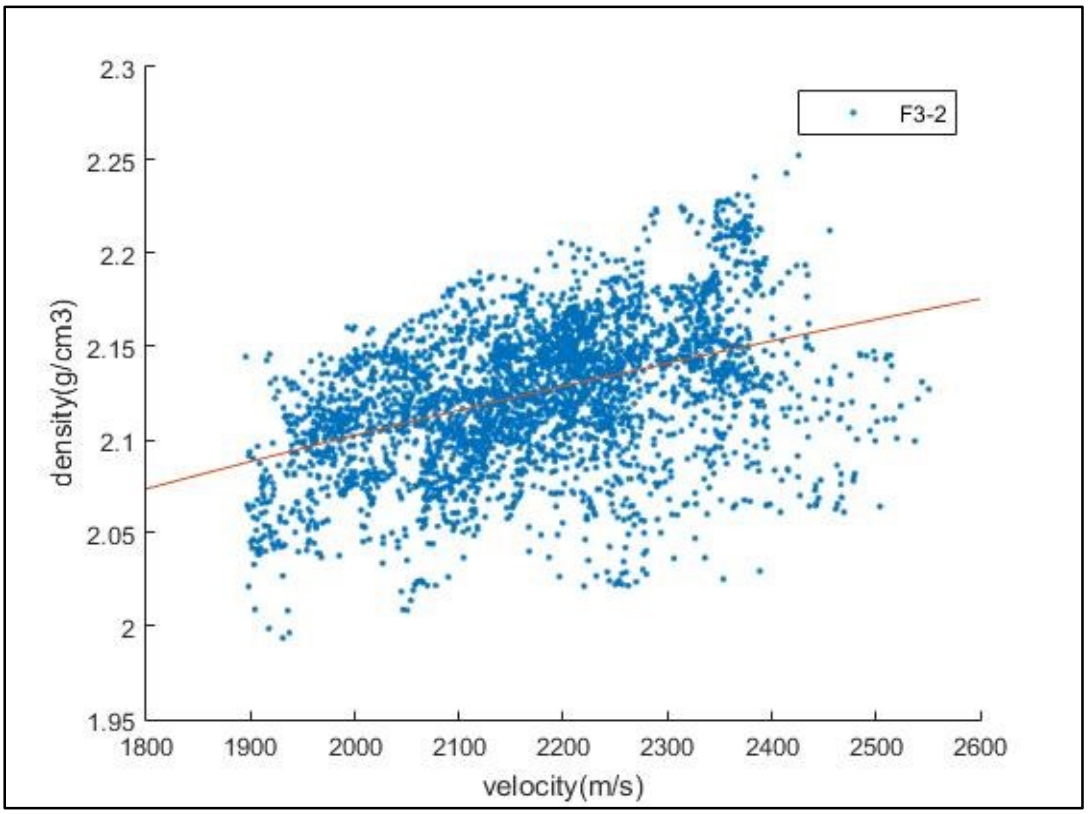

Figure 3.26. Cross plot of the density log against velocity log of the well F3-2 and simulate the density-velocity relationship based on the Gardner equation: $\rho = 0.7797V^{0.1305}$.

3.5.2. Acoustic impedance–Porosity

In this study, we have obtained three different density-velocity relationships in total. Next step is to determine which relationships should we use and how to use.

From Figure 3.27, the data range of well F3-2 is in the high-stand system tract (shale-prone) of the large scale sigmoidal bedding, and the shaly rocks seem fairly uniform. So for the high-stand system tract, the density-velocity relationship is from the well F3-2: $\rho = 0.7797V^{0.1305}$.

On the other hand, well F2-1 can be separated into two parts, with the upper part in the low-stand system tract (sand-prone) and the lower part is in the underlying horizontal sediment layers which we can see in more detail in Figure 3.28. The border of the low-stand system tract and the lower part is around 925ms.

Our target zone, the high amplitude seismic events, is in the low-stand system tract. However, there we have two different density-velocity relationships derived from the well F2-1. In order to choose the relationship for the low-stand system tract, we plot gamma ray with two-way travel time (a log displayed in time rather than depth), shown in Figure 3.29. For two-way travel time smaller than 925ms, the gamma ray value is mostly larger than 50 API, and we use the density – velocity relationship for the gamma ray > 50 API: $\rho = 0.1355V^{0.3569}$.

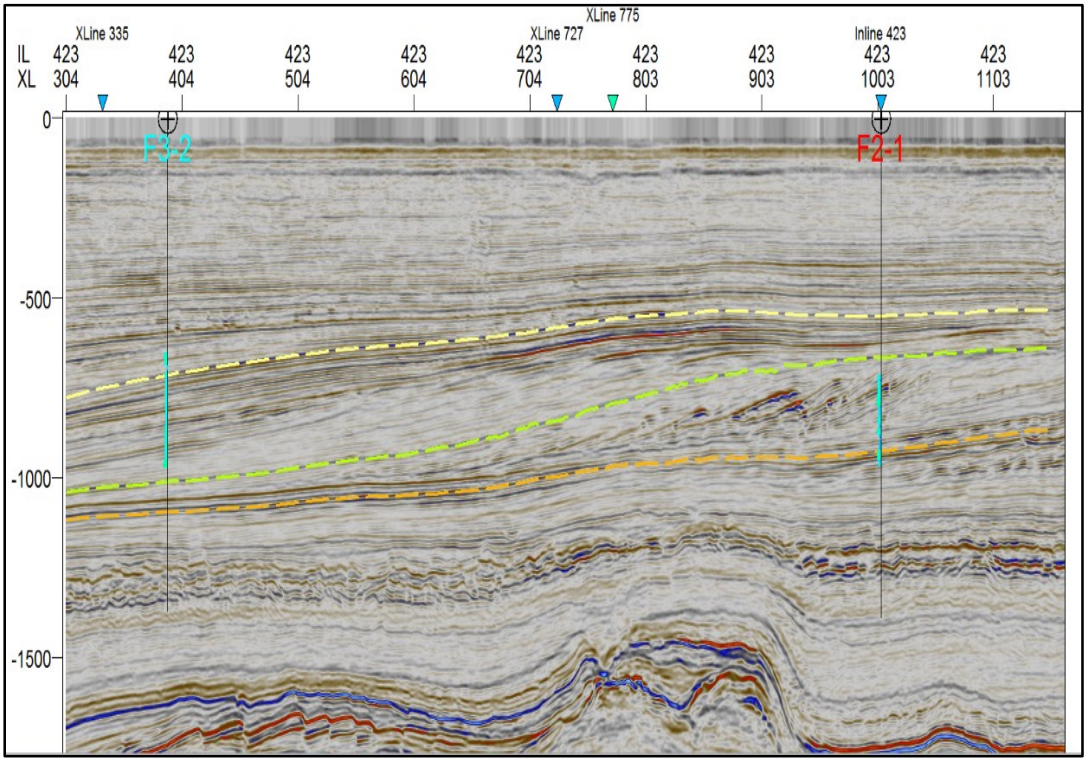

Figure 3.27. One seismic inline section and two wells displayed in one inline section. The boundary of the high-stand system tract and the low-stand tract are based on the tracked horizons.

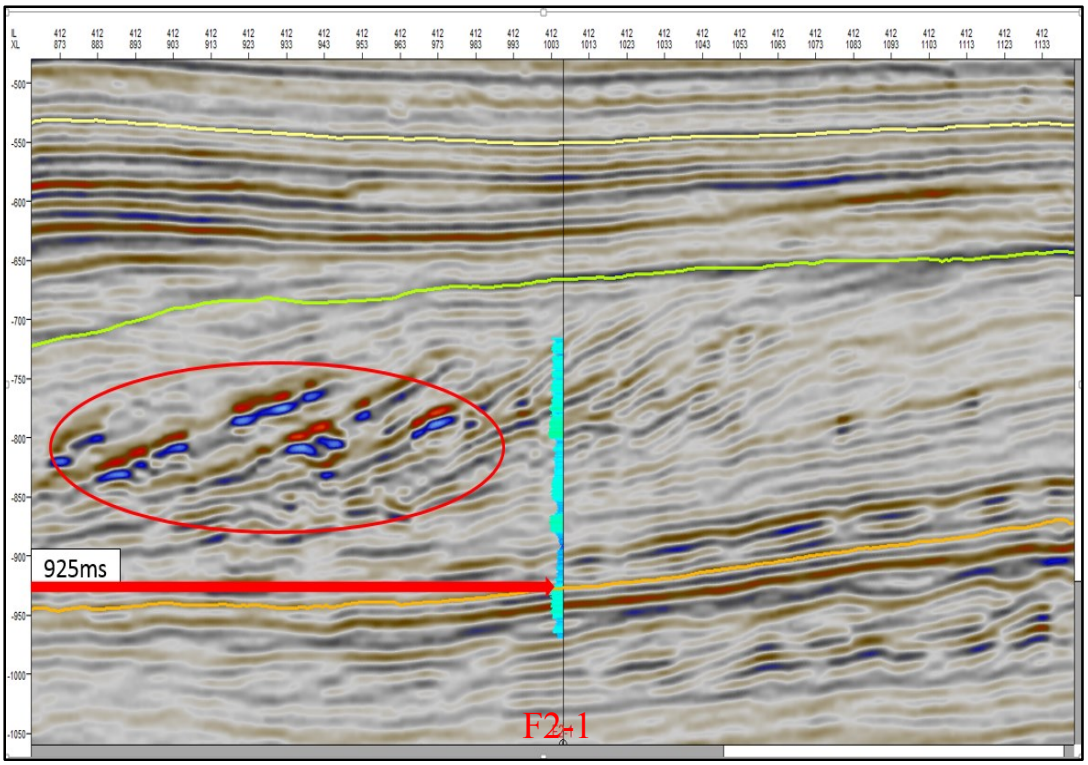

Figure 3.28. The well of F2-1 shown in time phase. The lower boundary for the low-stand system tract in the well F2-1 is 925ms. There are some high amplitude seismic events, circled in red, identifying our target zone.

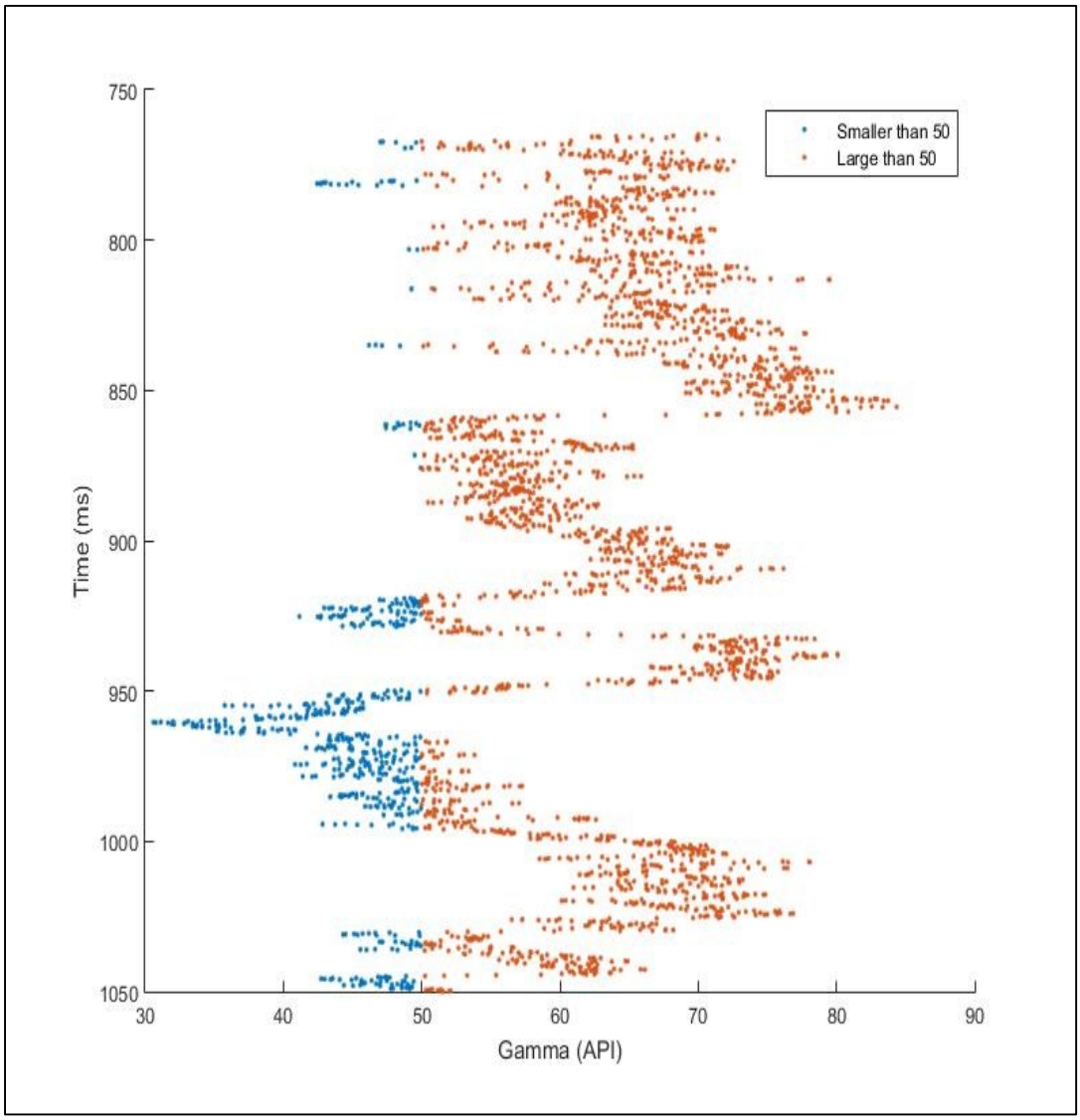

Figure 3.29. Log plot of Gamma ray in time domain for the well F2-1.

After obtaining the relationship between density and velocity, we can construct the relationship between the acoustic impedance and porosity through several steps:

- As the acoustic impedance is the multiply of density and velocity, we can use the velocity to represent the acoustic impedance.
- The porosity log is calculated from the density, so the porosity can also be represented by velocity.
- Since all the terms above can be represent by the velocity, a relationship between acoustic impedance and porosity can be constructed by the velocity.

So from the two density-velocity relationships, two acoustic impedance are achieved, respectively.

For the high-stand system tract:

$$AI = 0.7797V^{1.1305}$$

$$\emptyset_{DEN} = \frac{2.65 - 0.7797V^{0.1305}}{2.65 - 1.05}$$

$$\emptyset_{DEN} = -0.5015AI^{0.1154} + 1.656$$

For the low-stand system tract:

$$AI = 0.1355V^{1.3569}$$

$$\emptyset_{DEN} = \frac{2.65 - 0.1355V^{0.3569}}{2.65 - 1.05}$$

$$\emptyset_{DEN} = -0.1433AI^{0.263} + 1.656$$

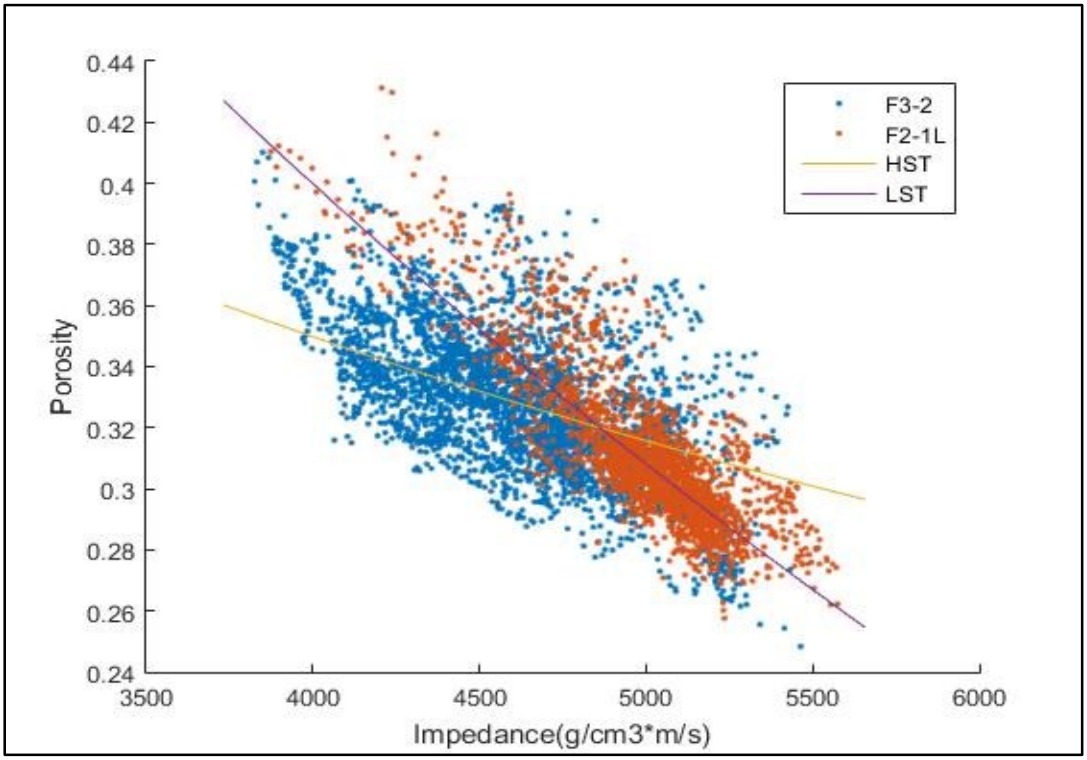

Figure 3.30. Cross plot of acoustic impedance against porosity and a relationship constructed by velocity. The blue dots represent the acoustic impedance and porosity log data in the well F3-2. The orange dots represent the acoustic impedance and porosity log data in the well F2-1. The yellow line is the linear relationship of the impedance and porosity which was developed by velocity from the well F3-2; this relationship would be reliable for the porosity prediction of the high-stand system tract. The purple line is the linear relationship of the impedance and porosity which was developed by velocity from the well F2-1; this relationship would be reliable for the porosity prediction of the low-stand system tract.

4. Results and Discussion

Since we have obtained two different seismic inversion models (deterministic inversion and stochastic inversion) and two different acoustic impedance-velocity relationships for high-stand system tract and low-stand system tract, respectively, four different high resolution porosity models are generated, shown in figure 4.1.

Our target zone in the low-stand system tract shows several high porosity zones embedded in the low porosity zone. This is a good indicator for gas and oil reservoir. The apparent low porosity could be due to actual low porosity, or it could be due to lighter fluids present in the pores, since gas or light oil will reduce the acoustic impedance.

Comparing the porosity models from deterministic inversion model and the porosity models from the stochastic inversion model, the area of high porosity zone from the deterministic inversion is smaller than the area of high porosity zone from the stochastic inversion.

As various areas have different density-velocity relationship, so the acoustic impedance-porosity are also different in different system tracts. When we predict the porosity, each depositional system should be treated individually and analyze the results together.

Since the porosity is not necessarily accurate at the well location, the porosity for the low-impedance area may not be accurate. But we can still use these porosity models to pick the high porosity zone or define the porosity boundary.

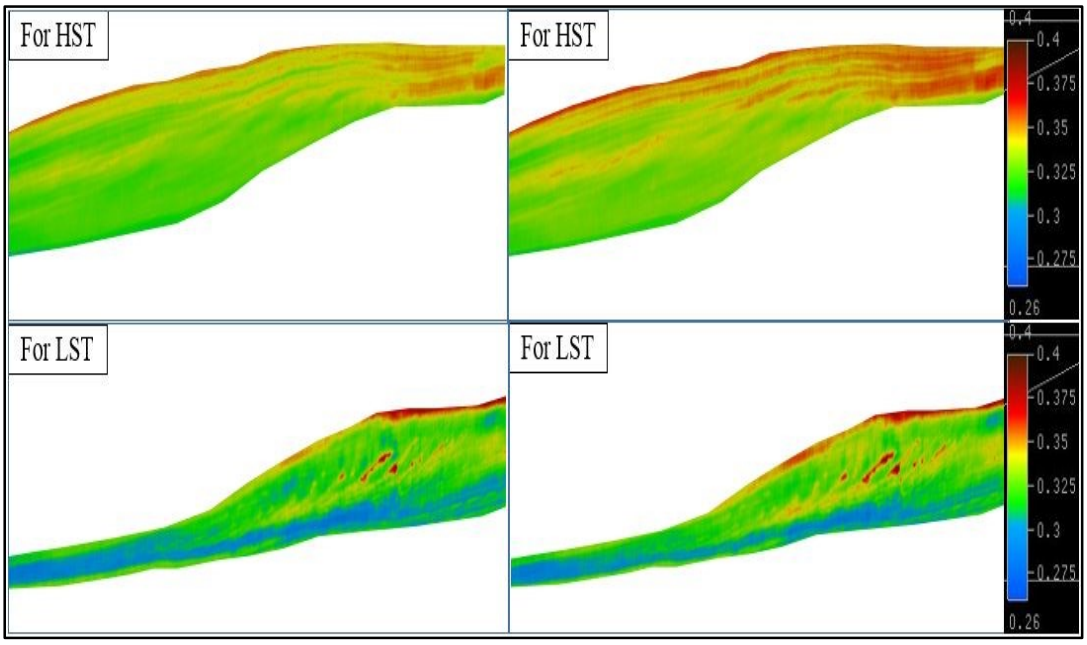

Figure 4.1. Porosity models converted from acoustic impedance inversion model. Top left is the porosity model of high-stand system tract from the deterministic inversion. Top right is the porosity model of low-stand system tract from the stochastic inversion. Bottom left is the porosity model of low-stand system tract from the deterministic inversion. Bottom right is the porosity model of low-stand system tract from the stochastic inversion.

5. Conclusion

Combining the reasonable low frequency model and the accurate estimated wavelet, two high resolution and reliable acoustic impedance models have been generated. By applying Gardner's equation in the density-velocity analysis, we have developed the acoustic impedance-porosity relationship from the log data. The inversion result can be directly converted to a porosity model and we can use that to predict the porosity for the non-well area, of course, including our target zone, but the porosity value may not be accurate due to assumptions that went into creating the initial porosity logs. According to our analysis of the acoustic impedance models and porosity models, we conclude that the target zone within the sigmoidal bedding, shown as high-amplitude events, are caused by low impedance, and that low impedance might be due to high porosity or to the presence of hydrocarbons. We further conclude that this target zone is likely to contain potential hydrocarbon reservoirs because the high-porosity zone is covered by a low-porosity zone, which is necessary for hydrocarbon traps. Both the deterministic inversion and stochastic inversion methods have been applied in this study; comparing these two inversion results showed that deterministic inversion tends to provide a smaller estimate for the volume of the potential reservoirs. In addition, because different areas may have various density–velocity relation, we recommend that considering both the high-stand system tract porosity model and the low-stand system tract porosity model in the

analysis for porosity of the entire sigmodal bedding zone is useful to achieve a more valid result.

References

Barclay, F., Bruun, A., Rasmussen, K. B., Alfaro, J. C., Cooke, A., Cooke, D., and Roberts, R., 2008, Seismic inversion: Reading between the lines: *Oilfield Review*, **20**, no.1, 42-63.

Cooke, D., and Cant, J., 2010, Model-based Seismic Inversion: Comparing deterministic and probabilistic approaches: *Canadian Society of Exploration Geophysicist Recorder*, **35**, 28-39.

Francis, A., 2005, Limitations of deterministic and advantages of stochastic seismic inversion: *Canadian Society of Exploration Geophysicist Recorder*, **30**, 5-11.

Hampson, D., and Russell, B., 1984, First break interpretation using generalize linear inversion: *54th Annual International Meeting, Society of Exploration Geophysicist, Expanded Abstracts*, 532-534.

Hasanusi, D., Adhitiawan, E., Baasir, A., Lisapaly, L., and Van, E. R., 2007, Seismic inversion as an exciting tool to delineate facies distribution in Tiaka carbonate reservoir, Sulawesi-Indonesia: 31st *Proceedings of the Annual Convention – Indonesian Petroleum Association*, **31**, 493-506.

Keys, J., R. and Forster, D., J., 1998, A data set for evaluating and comparing seismic inversion methods, in: Keys, J., R., and Forster, D., J., Comparison of Seismic Inversion Methods on a Single Real Data Set: *Society of Exploration Geophysicist,* 1-12.

Moyen, R., and Doyen, P. M., 2009, Reservoir connectivity uncertainty from stochastic seismic inversion: *79th Annual International Meeting, Society of Exploration Geophysicist, Expanded Abstracts*, 2378-2382.

Peterson, R. A., Fillippone, W. R., and Coker, F. B., 1955, The synthesis of seismograms from well log data: *Geophysics*, **20**, no. 3, 516-538.

Schroot, B. M., and Schuttenhelm, R. T. E., 2003, Expressions of shallow gas in the Netherlands North Sea: *Netherlands Journal of Geosciences*, **82**, no.1, 91-106.

Stefan, M., 1999, Variogram analysis of magnetic and gravity data: *Geophysics*, **64**, no. 3, 776-784.

Verma, A., Shuklal, N., Tyagi, S., and Mishra, N., 2014, Stochastic modeling and optimization of multi-plant capacity placing problem: *International Journal of Intelligent Engineering Informatics*, **2**, 139-165.

Xi, X., Ling, Y., Zou, Z., Sun, D., Lin, J., Wang, J. and Wang, H., 2013, The application of a low-frequency model constrained by seismic velocity to acoustic impedance inversion: *83th Annual International Meeting, Society of Exploration Geophysicist, Expanded Abstracts*, 3278-3282.